Technische Universität Braunschweig

Institut für Flugzeugbau und Leichtbau
IFL

VOLT AIRS 95

DLR Design Challenge 2024

Project Team

C. Dietrich
A. Kobeshavidze
L. Thiesen (Team lead)
G. Gutaj
M. Rasch
A. Vorndran

Acadedmic Advisors

Prof. Dr.-Ing. I. Staack

R. Y. Yanev, M. Sc.

Submitted on 21st July 2024

Abstract

VoltAirs-95 is a short-haul aircraft concept designed for 95 passengers. Carefully engineered as proposal for the DLR Design Challenge 2024 requirements, the concept features details regarding the aircraft's configuration, technical specifications and a life cycle analysis. The evaluation of the operational target parameters DOC and energy efficiency is carried out in comparison with a conventional *DASH-8-Q400* powered by 100 % sustainable aviation fuel (SAF).

The foundation for the development the *VoltAirs-95* is an in-depth analysis of the airport and route network provided by the challenge specifications. Based on that data, the selection process is conducted by a multidisciplinary methodical ranking of potential designs within the given constraints. Emphasis is put on a realistic, achievable configuration rather than over-ambitious and illusory designs and technologies to ensure the planned entry into service in the year 2050. The key element of the *VoltAirs-95* is its distributed electric propulsion powered primarily by batteries, allowing for greatly reduced climate impact and aggressively increased efficiency. To address the range limitations of battery electric aircraft, the concept incorporates a turboshaft-generator combination powered by SAF, which also helps to provide the additional energy required for eventual diversions or loiter phases. The new technologies applied result in an ultra-efficient and environmentally friendly aircraft with high passenger comfort. Despite the additional system complexity, the DOC increases only moderately by about 9 %.

Kurzfassung

VoltAirs-95 ist ein revolutionäres Kurzstreckenflugzeugkonzept für 95 Passagiere. Speziell für die DLR Design Challenge 2024 entwickelt, setzt es neue Maßstäbe in Sachen Energieeffizienz und maximaler Reduktion von Emissionen. Mit herausragender Leistung und optimierter Lebenszyklusanalyse eröffnet *VoltAirs-95* den Weg für einen nachhaltigen, grünen Luftverkehr innerhalb Europas und auf weltweiten Kurzstrecken. Die Einordnung der Zielparameter Betriebskosten und Energieeffizienz erfolgt im Vergleich mit einer konventionellen *DASH-8-Q400*, die vollständig mit SAF betrieben wird.

Die Entwicklung von *VoltAirs-95* basiert auf einer detaillierten Anforderungsanalyse des vorgegebenen Streckennetzes, die die Bewertungsgrundlage für eine methodische Bewertung aller potentiellen Technnologien und Konfigurationsalternativen schafft. Das gewählte Konzept zieht die realistische Machbarkeit einer zu ehrgeizigen Konfiguration vor, um die geplante Inbetriebnahme im Jahr 2050 sicher zu gewährleisten. Schlüsselelement von *VoltAirs-95* ist ein batteriegespeister verteilter elektrischer Antrieb, der die Emissionen deutlich reduziert und die Effizienz erhöht. Um die begrenzte Reichweite von batterieelektrischen Flugzeugen auszugleichen, verfügt das VoltAirs-95 über eine mit nachhaltigem Luftfahrtkraftstoff betriebene Turbinen-Generator-Kombination ("Range-Extender"), die die gegebenenfalls zusätzlich benötigte Energie für einen Ausweich- und Warteflug bereitstellt. Während die neue Konfiguration und die neuen Technologien ein äußerst effizientes und umweltfreundliches Flugzeug ermöglichen, führen diese zu einem moderaten Anstieg der Betriebskosten um etwa 9 %. Ein echter Meilenstein in der Luftfahrt!

Team Members

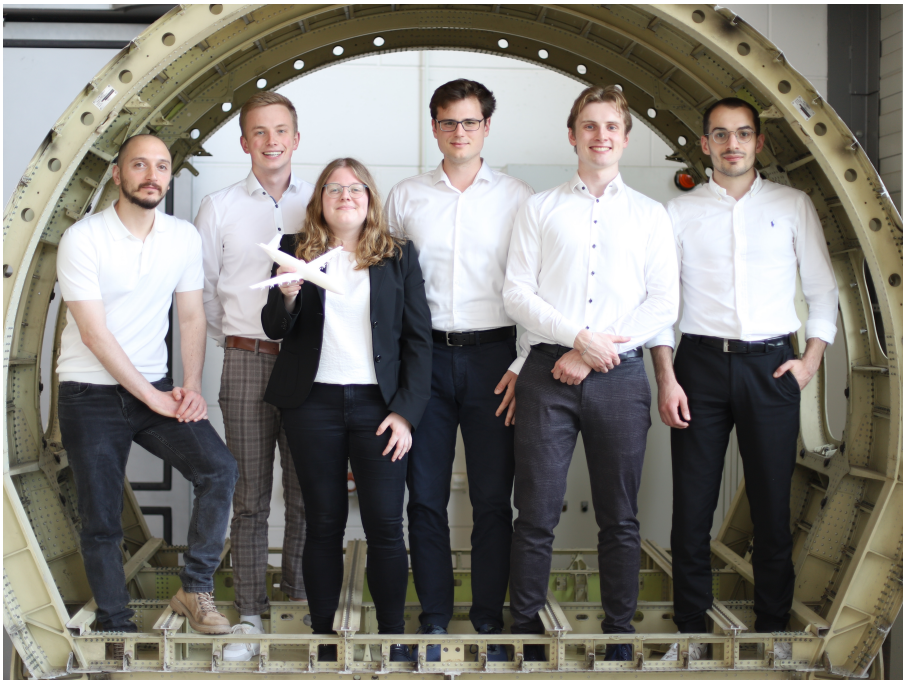

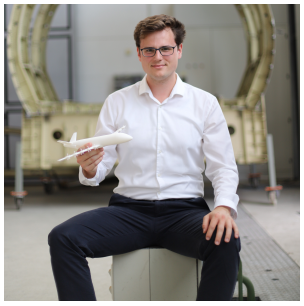

Christian Dietrich
2nd Master Semester
Aerospace Engineering

Gent Gutaj
2nd Master Semester
Aerospace Engineering

Aleksandre Kobeshavidze
2nd Master Semester
Aerospace Engineering

Mika Rasch
2nd Master Semester
Aerospace Engineering

Lukas Thiesen
2nd Master Semester
Aerospace Engineering

Anna Vorndran
3rd Master Semester
Energy Engineering

Technische Universität Braunschweig

Institut für Flugzeugbau und Leichtbau
IFL

Technische Universität Braunschweig | Institut für Flugzeugbau und Leichtbau
Hermann-Blenk-Straße 35 | 38108 Braunschweig | Deutschland

Technische Universität
Braunschweig
Institut für Flugzeugbau und Leichtbau

Hermann-Blenk-Straße 35
38108 Braunschweig
Deutschland

Prof. Dr.-Ing. Ingo Staack
M.Sc. Radimir Y. Yanev

Tel. +49 (0) 531 391-9936
r.yanev@tu-braunschweig.de
http://www.tu-braunschweig.de/ifl

Datum: 17.07.2024

Confirmation for submission

The submitted project has been approved by the head of the Institute of Aircraft Design and Lightweight Structures (IFL) and is approved for submission to the DLR Design Challenge 2024. The work has been carried out independently by the following six students currently enrolled at the Technische Universität Braunschweig:

Mr. Christian Dietrich
Mr. Gent Gutaj
Mr. Aleksandre Kobeshavidze
Mr. Mika Rasch
Mr. Lukas Thiesen
Ms. Anna Vorndran

Technische Universität Braunschweig
Institut für Flugzeugbau und Leichtbau
Prof. Dr.-Ing. Ingo Staack
Hermann-Blenk-Straße 35
38108 Braunschweig

Prof. Dr.-Ing. Ingo Staack

R. Y. Yanev

Radimir Y. Yanev

Contents

List of Figures

List of Tables

Nomenclature

Abbreviations

AEO	All Engines Operative
ANC	Active Noise Control
BMS	Battery Management System
BT	Block Time
BTMS	Battery Thermal Management System
CC	Constant Current
CFRP	Carbon Fibre Reinforced Plastic
CG	Centre of Gravity
DEP	Distributed Electric Propulsion
DOC	Direct Operating Cost
ECS	Environmental Control System
EHA	Electro-Hydrostatic Actuator
EIS	Entry Into Service
EM	Energy Mass
EoL	End of Life
FT	Fuel Tank
GHG	Greenhouse Gas
GWP	Global Warming Potential
HX	Heat Exchanger
HEFA	Hydroprocessed Esters and Fatty Acids
HPP	Hydraulic Power Pack
LCA	Life Cycle Assessment
Li	Lithium
LRU	Line Replaceable Unit
MC	Maintenance Cost
MLM	Maximum Landing Mass
MPLM	Maximum Payload Mass
MTOM	Maximum Take-off Mass
MZFM	Maximum Zero Fuel Mass
NLF	Natural Laminar Flow
NMC	Nickel Manganese Cobalt Oxide
OAT	Outside Air Temperature
OEI	One Engine Inoperative
OEM	Operational Empty Mass
PAX	Passenger
PCU	Power Control Unit
PTC	Positive Temperature Coefficient
RAT	Ram Air Turbine

RE Range Extender
SAF Sustainable Aviation Fuel
SDG Sustainable Development Goals
SoC State of Charge
TRL Technology Readiness Level
UN United Nations

Symbols - 1

Symbol	Description	Unit
A_{Wing}	Wing Area	m^2
AR	Aspect Ratio	–
A_V	V-Tail Area	m^2
b	Wingspan	m
BT	Block Time	h
$BT_{stopover}$	Stopover Block Time	h
$BT_{nonstop}$	Nonstop Block Time	h
C_D	Drag Coefficient	–
C_{Di}	Induced Drag Coefficient	–
C_{D0}	Zero-lift Drag Coefficient	–
C_L	Lift Coefficient	–
$C_{L_{\mathrm{LD}}}$	Lift Coefficient Landing	–
$C_{L,max}$	Maximum Lift Coefficient	–
C_{L}-α	Lift Curve Slope	1/rad
C_{M}-α	Moment Coefficient	–
c_i	CO_2 – equivalents	$\mathrm{kgCO_2 - eq./kg_i}$
c_i^{spez}	Specific CO_2 Equivalent	$\mathrm{kgCO_2 - eq./MJ_i}$
$DOC_{p.PAX}$	DOC per PAX	$/PAX
DOC_{tot}	Total DOC	$
e_{Bat}	Battery Energy Density	Wh/kg
e_{SAF}	SAF Energy Density	Wh/kg
FC	Flight Cycles per Year	–
$f_{stopover}$	Share of Flights with Stopover	%
g	Gravitational Acceleration	m/s^2
L/D	Lift to Drag Ratio	–
$h_{U,i}$	Lower Heating Value	MJ/kg
$I_{(dis)charge}$	(dis)charging Current	A
Ma	Mach-Number	–
$OT_{p.a.}$	Operational Time per Year	h
Q_{Bat}	Battery Storage Capacity	Ah
R	Flight Range	km
v	Average Cruise Speed	km/h
V_A	Design manoeuvre Speed	km/h
V_C	Design cruise Speed	km/h
V_D	Design dive Speed	km/h
V_F	Max Speed with flaps deployed	km/h
$\mathrm{V_{stall,LD}}$	Stall Speed landing Configuration	km/h
$\mathrm{V_{stall,T/O}}$	Stall Speed take-off Configuration	km/h
V_{S1}	Stall Speed clean Configuration	km/h
V_{S0}	Stall Speed landing Configuration	km/h
x_i	Emitted GHG	kg

Symbols - 2

Symbol	Description	Unit
α	angle of attack	$^\circ$
η_{bat}	Battery Efficiency	–
η_{gen}	Generator Efficiency	–
η_{RE}	Range Extender Efficiency	–
η_{elec}	Efficiency of electrical Powertrain	–
η_{prop}	Propeller Efficiency	–
η_{Turb}	Gas Turbine Efficiency	–
ρ	Density	kg/m^3
ϕ_{25}	Sweep at 25 % Chord Line	$^\circ$
ν	V-Tail Dihedral	$^\circ$

1 Introduction

Climate change is one of the greatest challenges that humanity is facing in the 21^{st} century. The adverse effects of global warming, caused primarily by greenhouse gas emissions from hydrocarbon fuels, have far-reaching environmental, social and political consequences [1]. Current fossil kerosene-powered aircraft are estimated to contribute 4 % to anthropogenic climate change, and their impact is expected to increase significantly in future [2]. International policymakers and the aviation industry have recognised the urgent need for a radical change and have set a goal of achieving net-zero carbon emissions by 2050 [3, 4]. A crucial element in the pursuit of this goal is the development of aircraft powered by sustainable energy sources for the regional air transport market [5]. This year's DLR Design Challenge invites students to rethink regional air transportation and design an aircraft that meets future demands in environmental impact and economically efficiency.

The six-member student team from TU Braunschweig faced the challenge and hereby presents their proposal of a future solution of sustainable regional air travel. *VoltAirs-95* is an innovative 95-passenger (hybrid-)electric aircraft with a range of 894 km designed to cut energy consumption by halve, reduce CO_2 emissions by 94 % and enhance passenger comfort compared to state-of-the-art regional transport aircraft. The following report presents the design process, aircraft features, technical specifications and concept of operation to demonstrate the feasibility of *VoltAirs-95*'s Entry Into Service (EIS) 2050.

2 Preliminary Design Process

Prior to the aircraft design phase, preliminary design considerations are made to decide on an aircraft concept. After analysing current short-haul aircraft, methodical approach is employed to identify the most practical overall configuration to meet the requirements extracted from the problem analysis. Having decided on *VoltAirs-95*'s configuration, the optimal design point for the given network of routes is established.

2.1 Current Configurations for short-haul Aircraft

To date, kerosene-based aircraft operate the regional air transport market. Examples of conventional short-haul aircraft are the *Embraer E-Series*, the *Bombardier CRJ900*, the *Fokker 100*, the *ATR-72* and the *Dash-8-QSeries*. Although these aircraft serve similar routes, they differ significantly in size and configuration. Furthermore, a large share of these routes is operated by *Airbus A320* or *Boeing 737* family aircraft, although these aircraft are optimised for much longer ranges. Despite their bigger cabin and suboptimal energy consumption, these aircraft are mainly used because of the operator's desire for flexibility and fleet homogenisation.
Table 2.1 gives a broad overview over the most important specifications of these aircraft. The *DHC-8-Q400* is eventually chosen as the reference aircraft, as it was found to be the closest to *VoltAirs-95* in terms of aircraft specifications. This is further detailed in section 5.4.

Table 2.1: Comparison of aircraft operating short-haul routes

A/C	*E190* [6]	*CRJ900* [7]	*ATR72* [8]	*DHC-8-Q400* [9]	Fokker 100 [10]
PAX	100	90	74	82	109
Range [km]	4445	3660	1540	2037	4300
MTOM [t]	51800	36514	22800	29574	44450
Cruise [km/h]	870	882	511	667	755

2.2 Methodical Concept Selection

In order to ensure objectivity of the decision on the optimal aircraft configuration, a methodical approach in the style of methods proposed in *VDI 2221-1* [11] is applied.

Aircraft requirements
This year's DLR Design Challenge task is the design of a sustainable short-range aircraft with EIS in 2050. It will operate a hub-and-spoke network, connecting Hamburg Airport to 15 European airports.

The aircraft's maximum runway length must allow operation from smaller airports, high climb and descent angles are increased to reduce noise emissions. In order to operate at the airports of the given network, the wingspan is limited to 36 meters, as the maximum box size available at all airports is "C" [12, 13]. The average passenger mass (including luggage) is set to 95 kg. Range and cabin size are deliberately not specified in the task and will be subject to further analysis of the network in section 2.3 and 2.4. In addition, the aircraft must be able to perform a reserve mission. This consists of a 250 km diversion flight, half an hour of loitering and 5% energy contingency after landing. Table 2.2 summarises all required specifications.

Table 2.2: Design requirements from the DLR Challenge Task

Parameter	Value
Maximum runway length	< 1510m
Descend angle from 1000 m	$> 5,5°$
Climb angle up to 1000 m	$\geq 4,5°$
Reserve flight	250 km diversion + 30 min loiter + 5 % contingency

Morphological Analysis

To identify possible aircraft configurations that meet the requirements, a morphological analysis is carried out. First, the overall transport task is decomposed into several partial functions. Next, an extensive literature research is carried out to identify individual solutions that fulfil the defined sub-tasks. Table 2.3 shows an extract of the morphological box. The morphological box is used to generate five different aircraft configurations, combining the partial solutions and exploiting synergies.

Based on the list of requirements, 29 criteria are defined to evaluate different aircraft concepts. The criteria are divided into six sub-categories:

- Aerodynamic properties
- Structure and mass
- Ease of operation
- Energy source integration
- Propulsion system efficiency
- Overall configuration

For the decision-making process, a ranking of the criteria within each category is carried out by evaluating the importance of the criteria in relation to each other and assigning points. This produces a weighting factor for each criterion.

Table 2.3: Morphological box

Aircraft Component	Partial Function	Individual Solutions				
Fuselage	**Accommodate payload**	Cylindrical	Double-Bubble	Blended Wing Body	Windowless fuselage	
Wing	**Lift generation**	Low wing	High wing	Strut-based wing	Boxwing	Folded wingtips
	Drag reduction	Boundary layer extraction	Shock-bumps	Sharkskin	Winglets	Natural Laminar Flow (NLF)
Control	**Flight controls**	Elevator/rudder/ailerons	V-tail + aileron	Morphing Wing	T-Tail + aileron	
Powertrain	**Energy storage**	SAF	liquid hydrogen (LH_2)	gaseous hydrogen (GH_2)	Battery	
	Energy conversion	Fuel cell (PEM)	Fuel cell (SO)	Gas turbine (combustion)	Transformer	Recuperator
	Accommodation	Tail	Inside wing	Cargo deck	Pods (below wing)	
Drivetrain	**Generate thrust**	Distributed Electric Propulsion (DEP)	Open rotor	Propulsive fuselage	large propellers	Fan with high bypass ratio
	Generate shaft power	Gas generator	Electric motor	Magnet		

Concept Selection

Based on the conclusions from the technology literature research, each concept is assessed regarding the fulfilment of the criteria. A score ranging from one point to six points is awarded (higher scores indicate better compliance) and multiplied by the respective weighting factor. The results of this qualitative assessment are presented in Table 2.4.

Table 2.4: Possible configurations to satisfy the above mentioned requirements

Configurations	Fuselage	Wing and Aerodynamics	Control	Powertrain	Drivetrain	Total Score	Score in %
Configuration 1	Double-Bubble	Low wing, folded wingtips, Sharkskin	T-Tail, ailerons	100% Battery electric	DEP, propulsive fuselage	21.65	60.13
Configuration 2	Cylindrical, windowless	Low wing, winglets	V-tail, ailerons, morphing flap	Batteries, SAF powered gas turbine for range extension	DEP	22.83	63.42
Configuration 3	Cylindrical	High wing, folded wingtips, sharkskin, NLF	V-tail, ailerons	LH_2 tank behind cabin PEM-fuel cell in engine pod	2x electrically driven propellers	19.69	54.69
Configuration 4	Cylindrical	Strut-based wing, folded wingtips, sharkskin, NLF	T-Tail, ailerons	LH_2 tank behind cabin LH_2 powered turbine	2x ducted fans (tail drive)	22.16	61.55
Configuration 5	Cylindrical	Low wing, sharkskin, winglets NLF	V-tail, ailerons	LH_2 tank behind cabin PEM fuel cell (tail)	DEP	21.83	60.64

Configuration 2 achieves the highest total score of 63.13 %. The features of the configuration are shown in Figure 2.1. A decisive argument in favour of this concept compared to its hydrogen-based competitors is the higher convergence efficiency from the energy source to propulsion for the battery-electric powertrain [14]. This argument is even stronger when the conversion efficiencies for the production of green hydrogen are considered [14]. Beyond that, electric mobility has the advantage of requiring less refuelling infrastructure, making it easier to implement at small airports. Thus, configuration 2 achieves high scores in propulsion and operation. In addition to this, the layout with distributed electric propulsion, large wings and a V-tail results in favourable aerodynamics, making use of synergies. A final argument for this concept is the feasibility. As it employs a SAF-based RE as an additional power source on long flights, the concept allows more realistic battery density assumptions and requires less costly novel technologies compared to configuration 1. For these reasons, concept 2 is selected and evolved into the *VoltAirs-95* aircraft.

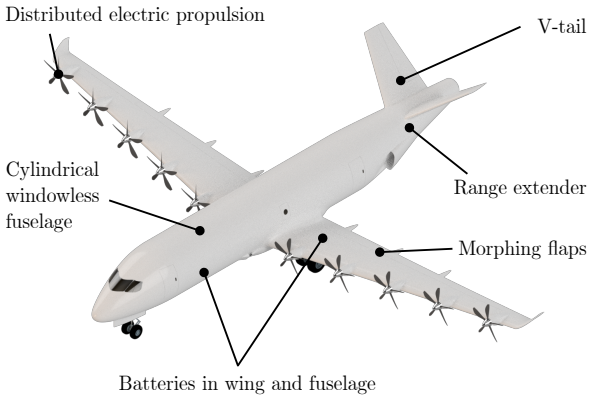

Figure 2.1: Features of Configuration 2

2.3 Route Network Analysis

To determine the optimum range and passenger capacity of the aircraft, the given network is analysed. The airport distances of the 17 connections vary between 361 and 1480 km. The four longest routes may be substituted by a one-stopover operation, thereby reducing the required mission range. Depending on the number of routes featuring a stopover (one to four), the aircraft ranges can be chosen as 894, 1095, 1188, 1250 or 1480 km. The demand is provided in Passenger (PAX) per week per connection, while each connection must be served at least two times per week. On routes with optional stopover, no passenger are meant to leave nor board the plane. The main hub of the network is Hamburg (HAM), where a maximum of 276 slots per week is available and least 142 slots must be used to serve the network. This limits the cabin size to be between 60 PAX and 124 PAX. With the given amount of PAX per week given for each connection, the required number of flights on each route can be calculated as a function of the aircraft's cabin size. The number of flights required for transporting all PAX are lower for bigger cabins, thus making a step if a flight can be omitted as shown in Figure 2.2. As the demand is specified to be static, the number of unsold seats per week can be assessed directly (compare red line in Figure 2.2). Generally, utilisation decreases for increasing cabin sizes, but exhibits some significant peaks at several cabin sizes due to the discrete and static number of passengers. Consequentially, the cabin size will be chosen to match one of these local optima.
With the number of flights per week, the number of aircraft required to operate the network can be calculated with the help of the utilisation formula from [15].

$$FC = \frac{OT_{p.a.}}{\left(\frac{R}{v} + BT\right)} \tag{2.1}$$

The number of flight cycles per aircraft per year FC depends on the range R, the average cruise speed v and the average Block Time (BT). $OT_{p.a.}$ is the operational time per year, equalling the difference of operated hours per year and the yearly forced downtime, statistically determined to 2748.8 h.

For the range, a reference mission is introduced by averaging the length of the individual connections, weighted with the number of passengers transported. The optimum cruise condition of 612.72 km/h at an altitude of 7 km is determined by an iterative process described in chapter 3, which considers aerodynamics, propulsion and Direct Operating Cost (DOC). For the BT calculation the value of [15] is adopted. The block time must be taken into account twice for flights with stopover.

$$BT_{stopover} = BT_{nonstop} \cdot ((1 - f_{stopover}) + 2 \cdot f_{stopover}) \tag{2.2}$$

The increase in block time for aircraft with smaller range shown in Table 2.5 is the reason why more aircraft are required to operate the network.

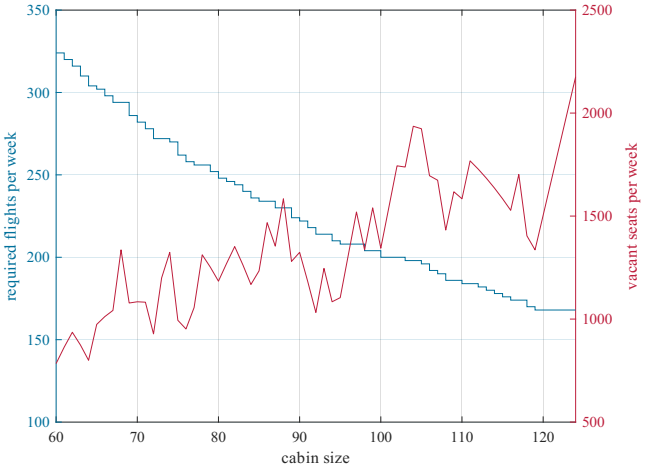

Figure 2.2: Required number of flights and unoccupied seats per week, for variable cabin sizes

The calculated number of aircraft required to operate the network decreases for bigger cabins, since less flights are necessary to transport all passengers. A detailed analysis of the cabin size on the aircraft's DOC is required to weigh up the decision between higher aircraft utilisation and fewer aircraft required to operate the network.

Table 2.5: Changes in block time for different aircraft ranges

Range	share of flights with stopover	relative block time
1480 km	0.0 %	100.0 %
1250 km	5.9 %	105.9 %
1188 km	12.2 %	112.2 %
1095 km	17.9 %	117.9 %
894 km	22.5 %	122.5 %

2.4 Determination of Design Point

The aircraft shall be tailored to the described route network and the target criteria, which are energy consumption per passenger kilometre and DOC. For this reason, preliminary considerations are made regarding the design variables payload, capacity, aircraft range and fraction of SAF-powered flight. To estimate the effect of these design variables, parameter variations are performed and the design objectives evaluated. As the determination of the design point and the aircraft preliminary design are iterative, any performance parameters needed for the calculation are chosen in accordance with considerations made in chapter 3 and 4.

Starting point for the parameter variation is a simplified aircraft sizing using a Class-I mass analysis and Breguet mission. For battery-electric flight, the mass of the energy source does not change through a reduced depth of charge during flight [16]. Therefore, the Breguet equation is adapted to estimate the energy mass fraction $\frac{M_{bat}}{M_{MTOM}}$ required to facilitate the battery-powered flight range [17].

$$R = \eta_{prop} \cdot \eta_{elec} \cdot e_{bat} \cdot \frac{1}{g} \cdot L/D \cdot \frac{M_{bat}}{M_{MTOM}} \tag{2.3}$$

The range is set by η_{prop} and η_{elec}, which describe the energetic efficiencies of the propeller and the electrical powertrain, the battery energy density e_{bat} and the aircraft's lift-to-drag ratio L/D. For the SAF-powered share of flight, the turbo electric Breguet equation for is employed to calculate the fuel mass fraction $\frac{M_{SAF}}{M_{MTOM}}$ [17].

$$R = -\eta_{prop} \cdot \eta_{elec} \cdot \eta_{gen} \cdot \eta_{turb} \cdot e_{SAF} \cdot \frac{1}{g} \cdot L/D \cdot ln\left(1 - \frac{M_{SAF}}{M_{MTOM}}\right) \tag{2.4}$$

The convergence efficiencies of the gas turbine η_{turb} and generator η_{gen}, as well as the SAF energy density e_{SAF} are included in the calculation. The total Energy Mass (EM) fraction is the sum of the battery and SAF mass fractions. Next, the OEM fraction is calculated according to a regression model by Torenbeek [18]. The Maximum Take-off Mass (MTOM) is taken as the sum of the three sub-masses OEM, EM and Maximum Payload Mass (MPLM).
This preliminary sizing is performed for various parameter combinations of design range, payload, and SAF

flight share. Subsequently, the trip energy consumption per passenger is calculated for each mission on the route network, again using the BREGUET-equations. The energy required for the take-off and climb is accounted for by adding a "lost range" to each mission, in accordance with TORENBEEK [19].

For the DOC analysis the model described in Section 5.3 is implemented. The DOC is calculated on an annual basis per aircraft. The masses and respective energy consumption are taken from the methods described above and varied for each possible cabin size. Another boundary condition is the number of flight attendants. [20] requires two flight attendants for cabin sizes up to 100 PAX and three for 101 and more. The network analysis aspects of unsold seats and the number of aircraft required is also considered by multiplying the DOC with the reciprocal occupancy rate, assuming that the operator has to bear the cost of the unsold tickets.

$$DOC = DOC_{\text{tot}} \cdot \frac{1}{\text{occupancy rate}} \tag{2.5}$$

To consider the required number of aircraft, the total number of PAX transported in the network per year is divided by the number of aircraft.

$$DOC_{p.PAX} = \frac{DOC}{PAX/\text{ aircraft}} \tag{2.6}$$

The results of the parameter variations for range and payload are shown in Figure 2.3. For greater clarity, the share of SAF-powered flight is kept zero at first. The variation shows that an aircraft with 894 km design range is superior in terms of energy consumption per passenger-kilometre, regardless of the maximum passenger number. This is conclusive, as an electric aircraft that is designed to supply the energy demand for the longest flight will have a vastly oversized battery on all shorter routes, which in turn increases the energy required due to greater aircraft mass. A smaller battery size for a shorter design range case is also the primary driver for the significantly lower DOC of the 894 km case. Therefore, both criteria suggest to set a design range of 894 km.

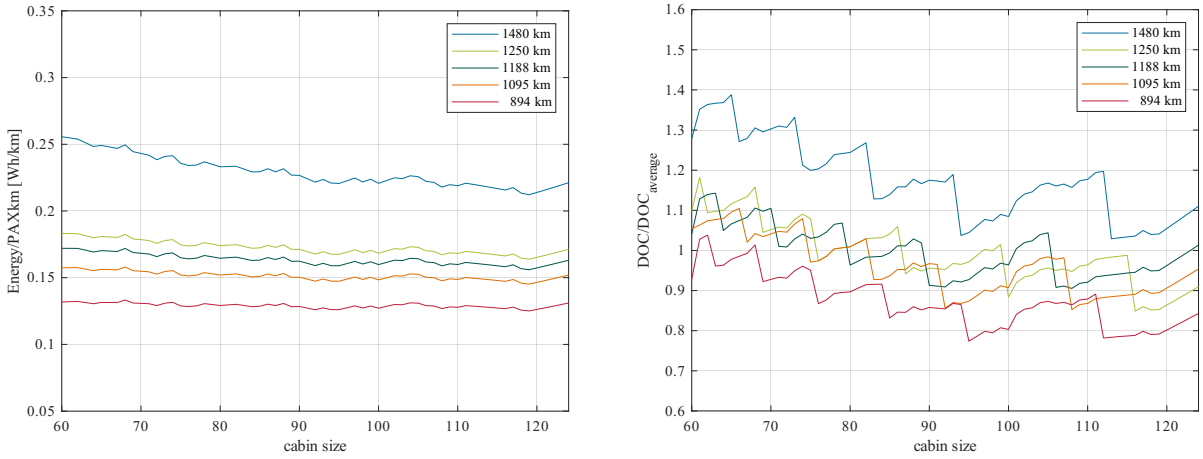

(a) Mission energy consumption

(b) Relative-DOC

Figure 2.3: Results of design range and payload variation - (SAF-share set to 0)

The cabin size exerts a minor influence on the energy consumption per passenger-kilometre, that are primarily caused by fluctuations in the occupancy rate. On the contrary, the DOC show a strong dependence. The DOC generally increase as the maximum payload increases since the capital cost of the aircraft and battery is directly related to the mass of the aircraft, which increases due to scaling effects. However, the graph shows several drops in DOC, when a smaller number of aircraft is required to operate the network, which significantly reduces the capital costs. The changes the occupancy rate of the cabin are also visible, but are less significant than other effects. Accordingly, the cabin size is selected to the global DOC optima, which is 95 passengers.

To determine the optimal share of SAF-powered flight, Figure 2.4 displays the normalised trend of both design objectives over the SAF-share for a 95 passenger aircraft with 894 km design range. Initially, the required energy decreases for increasing SAF-range, as the aircraft MTOM is reduced through storing more energy in an energy dense state. Due to the worse energetic efficiency of the turboelectric powertrain, especially the gas turbine, the energy demand increases for higher proportions of the flight covered by SAF.

It is evident that the DOC also changes with altering SAF-ranges. These changes are driven by the battery acquisition cost and the SAF energy costs. However, these aspects are mutually balanced and the relative variation is minor. The decision is made through a 50-to-50 weighting of both design objectives. The optimum lies at 19.5 % of the design mission (894 km + lost range), which equals 211 km cruise range. The diversion flight is chosen to be primarily SAF-powered, since it is not an actual part of the design mission and the impact on DOC and energy per PAX can therefore be neglected.

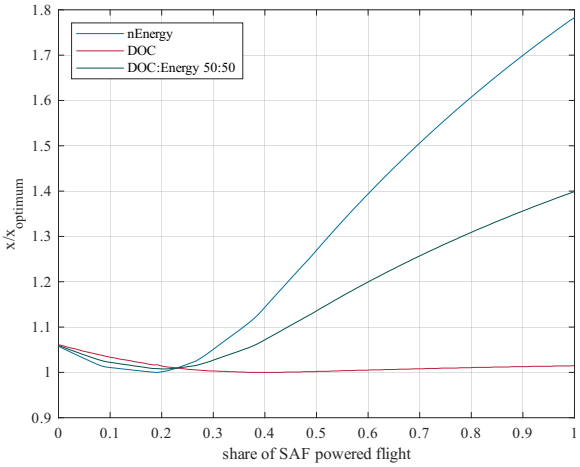

Figure 2.4: Results of SAF-share variation - ($R = 894\,\text{km}$, $N = 95\,\text{PAX}$)

3 Aircraft Configuration

VoltAirs-95 is a (hybrid-)electric short-haul aircraft for 95 passengers. It is propelled by ten electric motors distributed along the high-aspect ratio wing. The electrical energy is supplied by ten battery packs, installed into the wingbox and front fuselage cargo, and a SAF-powered range extension system. The aircraft's specifications are summarised in Table 3.1 and its dimensions are shown in the three-sided view Figure 3.1.

Table 3.1: *VoltAirs-95* specifications

Specification	Value
Cabin size	95 PAX
Propeller count	10
Wing area	83.38 m^2
Aspect ratio	13.08
MTOM	43 981 kg
Mission range	894 km
Diversion range	250 km
SAF-powered flight	19.5 %
Maximum shaft power	10 199 kW
Cruise glide ratio	20
Cruise speed	Ma 0.545
Cruise altitude	FL 230
Required runway length	1500 m
Climb rate	5.5°
Descent rate	5.7°

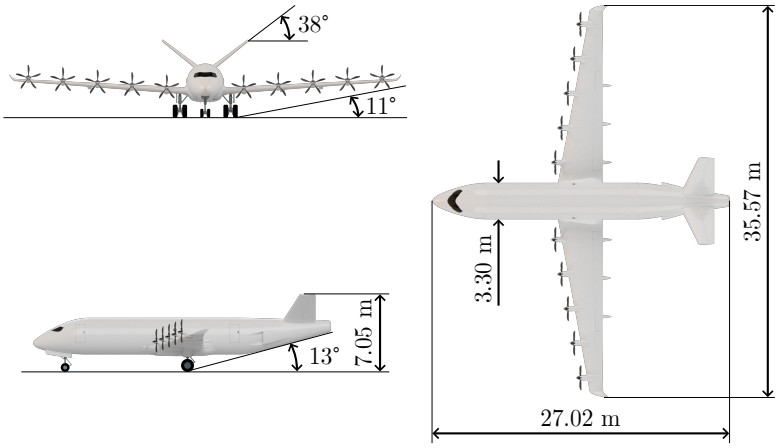

Figure 3.1: Three-sided view of *VoltAirs-95*

3.1 Fuselage and Cabin

The design of the fuselage is primarily driven by three objectives. The first is to contribute to good overall aerodynamic performance by minimising the fuselage's parasitic drag. The second is to reduce the fuselage weight, since a low OEM is key to the feasibility of a battery-electric aircraft. The final objective is to improve the passenger experience, which is a key selling point for airlines.

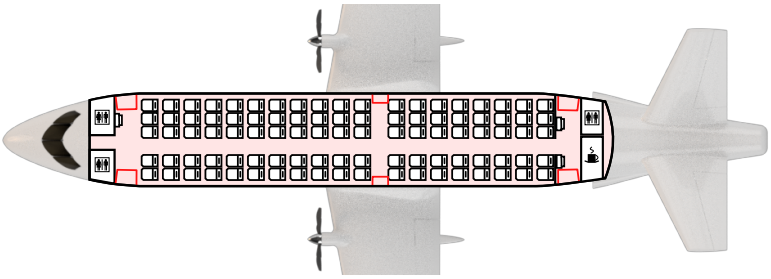

Figure 3.2: Proposed cabin layout

Several seating configurations were drafted and calculations show that a five-abreast seating arrangement gives the fuselage dimensions with the least wetted surface area. To reduce the fuselage length, an optimised compact design cabin layout, depicted in Figure 3.2 reduces empty space to an absolute minimum. With this design, 95 economy class seats with a 30 inch pitch can be installed in a fuselage of a total length of 27.02 m. Two *Type B* doors and one *Type III* hatch are distributed along the fuselage sides. For ease of airport operation, the door sizes chosen are larger than required byEASA emergency evacuation regulations [21].

Because the aircraft operation features flights with stopovers, the maximum time passengers spend on board is longer than on aircraft of comparable size. For this reason, more toilets are installed to meet passenger's personal needs. As the *VoltAirs-95* enters into service in 2050, a different kind of in-flight service is offered. Passengers will be able to select the beverages they wish to consume before flight and pick them up during boarding. This allows airlines to increase the variety of food on offer while minimising the number of unsold items carried on board. For flights with stopovers, the food supply can be replenished at the stopover-airport. Thus, the galley size is reduced to four full-sized trolleys.

The cabin features a windowless fuselage design. Instead, a virtual window system in the style of [22] is installed. It features external cameras flush-mounted into the fuselage structure and latest generation OLED-screens integrated into the cabin linings to provide artificial views for passengers. In addition to the virtual windows, the image data also enables new forms of in-flight entertainment, with the ability to broadcast the panoramic image to the passengers' personal virtual lenses. The elimination of fuselage openings and the surrounding support structure results in a simplified structural fuselage design with better fatigue performance and reduced manufacturing cost. Following the approach by [23], the reduction in structural weight is estimated at 164 kg. For regulatory reasons, the emergency exits continue to be fitted with real windows [21].

For propeller-driven aircraft, cabin noise reduction is an essential aspect for passenger comfort that needs to be addressed. According to [23], the windowless design is one contributor to reducing the noise induced into the cabin. In addition to this, an Active Noise Control (ANC) system is used, to cancel out the low frequency propeller noise through smart cabin linings in the style of [24]. In the futuristic cabin of the *VoltAirs-95*, passengers can connect their personal headphones to the aircraft ANC system to improve noise reduction even further.

3.2 Wing

Designing a wing for an energy efficient aircraft demands meticulous attention to various aerodynamic characteristics in order to achieve optimal performance. The low-wing configuration features a positive sweep of 5° and a dihedral of 4°, which works to stabilise any sideslip-induced roll moments, thereby enhancing the overall aerodynamic stability. Additionally, a negative twist of 2° from the wing root to the wingtips aids in improved stall management by ensuring that the stall progresses from the wing root towards the wingtips. This characteristic is critical for maintaining the effectiveness of control surfaces, even at high angles of attack. For the airfoil, the NACA 64-2-415 profile is selected for its ability to provide a suitable maximum lift coefficient, while also maintaining a good stall behaviour [25]. Moreover, the wing's relative thickness is carefully optimised, starting at 0.15 at the wing root and tapering to 0.12 at the wingtips.

High aspect ratio wing
Reducing the lift-induced drag is a significant aerodynamic benefit, as it contributes to approximately one-third of the total aircraft cruise drag for *VoltAirs-95*. For take-off and landing, the induced drag grows significantly, increasing approximately with the square of the lift coefficient (C_L). An effective measure to reduce the lift-induced drag is to increase the aspect ratio $AR = \frac{b^2}{A_{Wing}}$ [18], where b represents the span and A_{Wing} the wing area. The drag coefficient for the induced drag C_{Di} is calculated as displayed in Equation 3.1.

$$C_{\mathrm{Di}} = \frac{C_L^2}{\pi \cdot e \cdot AR} \tag{3.1}$$

The total surface area of the wing is 83.38 m^2, with a span of 35.57 m. This results in an aspect ratio of 13.08, which is slightly higher than that of the *Dash 8-Q400* with 12.8. Any further increase in this parameter would result in higher structural loads. The wing taper of 0.3 results in an improved lift distribution and decreases

the root bending moment. With the calculated OSWALD-efficiency factor of 0.89, a Lift-to-Drag ratio of 20 can be achieved in cruise flight. A detailed display on how this value is achieved will be explained in section 4.2.

Winglet
Winglets reduce induced drag by mitigating wingtip vortices, which are created by the pressure difference between the suction and pressure side of the wing. They work like an wing extension increasing the effective aspect without increasing the root bending significantly [26]. This reduces the total drag of the *VoltAirs-95* by 3% and leads to significant energy savings and lower operational costs.

High-lift system
While a small wing area results in lower skin drag, the short runway length required for landing necessitates a relatively high lift coefficient $C_{L_{\mathrm{LD}}}$, which favours a larger wing area. An elegant solution to this conflict is a FOWLER flap which increases the wing area during in take-off and landing [27].

As the mass of the battery remains constant, the landing configuration is comparatively heavy, and the aircraft mass can be assumed to be almost constant throughout the flight. When fully extended, the flap system increases the wing area by 12 m^2. By doing so, a lift coefficient of 2.6 during is achieved. The flap occupies 30 % of the total wing depth and provides a maximum flap angle of 40° during landing. The flap is located over 70 % of the wingspan.

High-lift flaps represent a significant source of noise. The majority is generated as a consequence of the formation of shear stress and gap vortexes, which flow off the side edges of the high-lift device. Studies show that through the implementation of a connection between the flap's side edge and the wing, the noise can be reduced by 5-13 dB, depending on the flap position [28]. The concentrated shear layer/vortex system would no longer flow over a side edge, thereby eliminating this source of noise. For this reason, the gaps in the longitudinal direction are modified as seen in Figure 3.3 for the continuous moulded layer flap CML . An innovative option to realise this design would be a flexible structure that connects the side edges of the FOWLER flap to the main-wing in accordance with [29]. The element between flap and wing deforms its structure to extend the flap and is connected to a fitting on both ends [29].

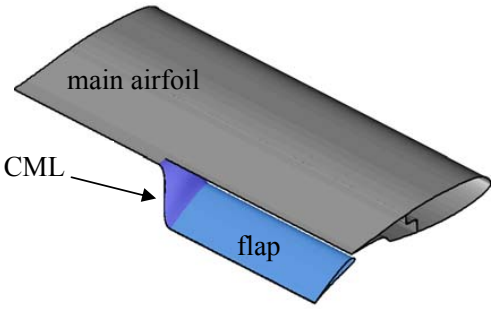

Figure 3.3: Continuous moulded layer flap [28]

3.3 Stability and Control

To reduce the interference drag of the aircraft, a V-tail is installed, combining the horizontal and vertical stabilisers into a single component. This leads to the minimisation of corners and edges. According to ROSKAM the drag for a V-tail is calculated in the same manner as for a wing [30]. Beyond that, a V-tail on an aircraft with fly-by-wire control does not lead to an increase in complexity compared to horizontal and vertical stabilisers [31]. The preliminary design process for the tail unit is divided into three distinct phases. The initial stage of the process is to design a horizontal stabiliser and ensure longitudinal stability. Subsequently, the vertical stabiliser is designed in accordance with lateral stability. This calculation takes into account the possibility of active lateral thrust compensation by the DEP, resulting in a reduced stabiliser area [32]. Finally, the individual tailplane components are integrated to form a V-tail configuration.

The V-tail is designed to provide longitudinal stability in cruise flight, while offering sufficient control. The wing profile exhibits a negative moment coefficient of -0.08 in cruise flight. The aspect ratio of the horizontal stabiliser and the volume factor are determined from statistical values according to the methodology described by manual methods. The longitudinal stability of *VoltAirs-95* is then verified to ensure that it remains within acceptable limits, given in [33]. In order to longitudinally trim the aircraft and maintain balance at different flight conditions, the Centre of Gravity (CG) can be dynamically adjusted by pumping fuel between the SAF fuel tanks.

Symbol	Description	Value	Unit
ν	Dihedral	37.76	[°]
A_V	Area	28,22	m^2
ϕ_{LE}	Leading Edge Sweep	10	[°]
l_μ	MAC	2,636	m

Table 3.2: Geometric parameters of the V-tail

To guarantee stability in the yaw and roll axes, statistical reference values have been selected for the vertical stabiliser. In the event of a critical engine failure, it is imperative that the vertical stabiliser can compensate for the additional yaw moment. Once it has been established that both the horizontal and the vertical tailplanes provide stability in the centre of gravity area, the V-tail is assembled from the individual parts. The vertical stabiliser can save 45 % of the surface area of the *VoltAirs-95* due to the active lateral thrust balancing.

The merging of the calculated horizontal and vertical surface areas results in the V-tail of *VoltAirs-95* with a dihedral of 37.76°. The geometric parameters are listed in Table 3.2. To calculate the dihedral the Equation 3.2 was used and for the area of the V-tail the Equation 3.3.

$$\nu = \arctan\left(\sqrt{\frac{A_{VTP}}{A_{HTP}}}\right) \tag{3.2}$$

$$A_V = \frac{A_{HTP} + A_{VTP}}{cos^2(\nu) + K * sin^2(\nu)} \tag{3.3}$$

Beyond that, *VoltAirs-95* flight controls feature an active load alleviation system. It is developed to manage and alleviate the aerodynamic forces acting on the structure, especially when gusts or turbulent conditions appear. As a consequence, the stress on the aircraft's structure during flight is reduced, allowing lighter structural dimensions [34]. Load alleviation system are already used in current aircraft's, such as the *Boeing 787 Dreamliner* and has benefit from a high technology readiness [35].

3.4 Distributed Electric Propulsion

Selection
At the selected subsonic cruise speed, propellers represent the most practical solution to generate thrust. They provide high efficiency, simplicity and low cost. By utilising a variable blade pitch, the propulsive efficiency can be maintained at a high level for the majority of flight segments, while also granting the capability of reverse thrust for deceleration upon landing. Recent advancements in the power densities of electric motors [36], coupled with their excellent scalability and reduced maintenance costs, present a promising alignment with propeller-driven aircraft. Consequently, electrically driven propellers are particularly suitable for the application of DEP, which enhances the overall aircraft characteristics in numerous ways:

1. In terms of aerodynamic advantage, DEP allows for a homogeneous distribution of thrust, resulting in local increases of dynamic pressure across the wing, increasing lift [37].
2. Thrust oversizing due to single engine failure cases is significantly reduced in comparison to a conventional twin-turboprop design. This effect propagates throughout the entire design and allows for reduced overall propulsion mass [38].
3. DEP reduces the total noise level generated by the powertrain [37].
4. The thermal loads are distributed in a less concentrated manner and can be handled more effectively.
5. Differential thrust may be applied in order to provide additional control of the yaw and roll axes. This enables an optimised empennage design, as described in section 3.3.

Design
VoltAirs-95 features ten laterally distributed, electrically driven five-blade propellers, with a shaft power of 1.03MW each, as discussed in detail in 4.3. The motors and power electronics are housed in streamlined nacelles, with the power electronics partially placed in the wing nose. The electric motors are air-cooled, due

to the low duration of the high-power segments and the sufficient air-speed in cruise flight. For the power electronics a separate liquid-cooling system is foreseen based on their location and increased heat generation. The liquid cooling ducts run through the wing's leading edge towards a main ram air heat exchanger, which is located in the belly fairing. The powertrain architecture is visualised in Figure 3.4.
The propulsive efficiency of $\eta_{\text{prop}} = 87\,\%$ and electric power transmission efficiency of $\eta_{\text{elec}} = 91.2\,\%$ (from battery to propeller shaft), are assumed in accordance with a comparable aircraft designs [14].

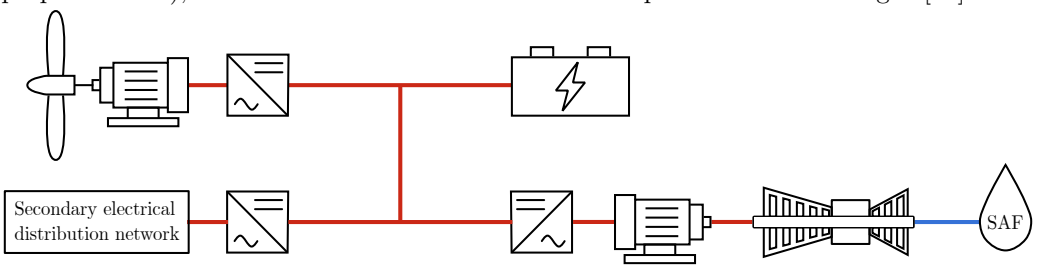

Figure 3.4: Powertrain architecture

3.5 Battery System

Rechargeable batteries have undergone a significant improvement during the last two decades and thus they already benefit from a very high TRL of 8 [39] and a high efficiency of $\eta_{bat} = 95\,\%$ [40, 41, 42]. Lithium (Li)-ion secondary batteries have virtually become the main energy storage in the large market of consumer electronics, and are currently the main zero-emission energy storage in the automotive industry. The automotive sector has enabled their price to decrease by 87 % during the second decade of the 21st century [43] and their application in the mobility sector is expected to grow significantly [44]. As the battery market is currently undergoing a radical change, the Li-battery might also be replaced by other promising battery technologies, such as the solid-state battery, in the near future. But since the *VoltAirs-95* concept is designed to be realistic, and other battery technologies are not yet well established, a reasonable Li-ion battery drive has been designed. [41]

Design of the aircraft battery system
The battery characteristics used for sizing the battery, such as cell and pack properties and operational ranges, are listed in Table 3.3. The battery parameters are based on new Tesla 4860 cell, which is implemented in the Tesla Model Y [45]. Currently, Nickel Manganese Cobalt Oxide (NMC) batteries have an gravimetric energy density of around 300 Wh/kg on cell level, but an annual increase of around 5 % is expected due to a strong research and development efforts, primarily from the automotive sector [16]. This would mean a energy density of more than 1000 Wh/kg on cell level by 2050. In order to take into account all subsystems that monitor and control the temperature of the battery as well as the housing of the battery cells, this value is decreased by 20 %. These parasitic losses lead to a system battery gravimetric energy density of 800 Wh/kg. [16, 46, 47, 48]

Table 3.3: Criteria for battery sizing

criterion	value
battery type [45]	NMC
cell shape	cylindrical
usable State of Charge (SoC)	15...85 %
upper SoC	<= 90 %
voltage of on-board power supply [49, 50]	800 V
cell rated voltage $U_{rated,cell}$ [45]	3.7 V
cell rated capacity $Q_{rated,cell}$ [45]	20 Ah
self-discharge rate	0 %
gravimetric energy density e_{grav}	800 Wh/kg
volumetric energy density e_{vol} [46, 51]	700 Wh/l

Unlike for fuel, not all of the energy capacity of the battery is available for propulsion purposes. *VoltAirs-95* battery is conservatively sized to use only 70 % of the nominal energy capacity, being discharged during flight between a SoC of 85 % to SoC of 15 %. One of the reasons for this is that a complete full charge (> 90 % SoC) and a deep discharge (< 5 % SoC) causes chemical reactions inside the cell that can possibly degrade the battery severely and thus shortens its service life significantly. Therefore, these charge ranges must be avoided if possible. [16, 42]
In addition, various types of resistance and loss mechanisms occur during operation. Thus, as the full capacity cannot be used as electricity, the battery is charged up to 90 % SoC to compensate for this losses during operation [14, 16]. Usually, lithium-ion batteries have a low self-discharge rate when stored, but as the aircraft will not normally have long idle times and is charged directly before take-off, this should be neglected here. The resulting battery, sized in accordance with literature procedures [40, 52] for the longest mission with a range of 894 km, contains 141,050 individual battery cells with a total mass of 12.98 tonnes and a volume of

14.91 m^3. To achieve the energy requirements of 7574 kWh for the longest battery-electric range and the peak power requirements (compare Chapter 4.3), the cells are electrically connected in a total of 217 cells in series and 650 cells in parallel (217s650p). For easier handling and safety considerations, the battery is divided into ten identical 217s65p packs (one per propeller). Four packs are placed in the fuselage, while the others are distributed along each wing. As depicted in Figure 3.5, each battery pack is divided into four equal sub-packs (Naming: Number of battery.Number of subpack) for ease of maintenance and positioning. The main Battery Thermal Management System (BTMS) components and the Heat Exchanger (HX) are located in the fuselage, while coolant is circulated to individual battery packs in the fuselage and wing, as seen in Figure 3.5.

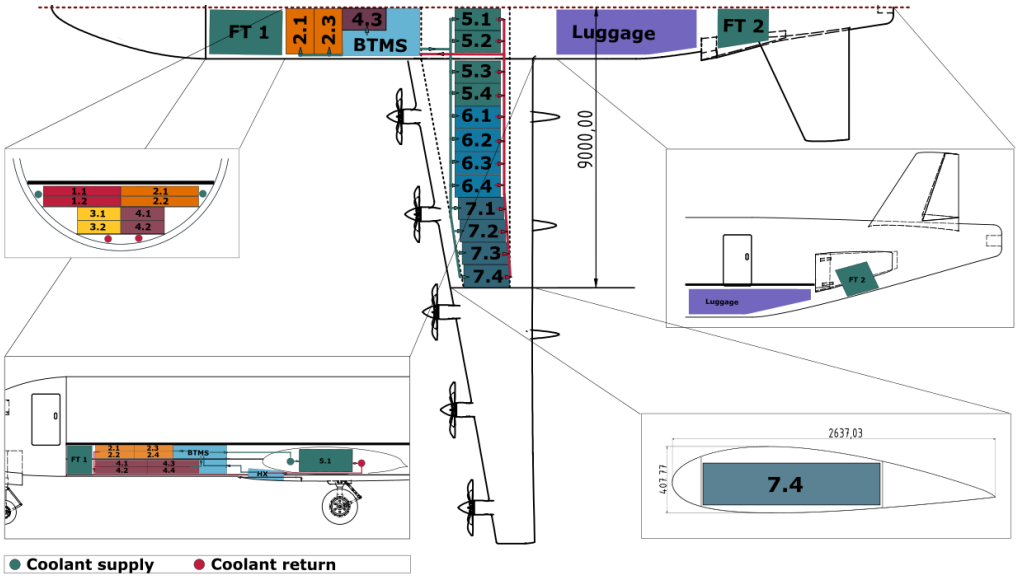

Figure 3.5: Schematic battery and BTMS positioning within the *VoltAirs-95*

Battery Management System and Battery Thermal Management System

When using a lithium-ion battery pack, it is essential to use a Battery Management System (BMS) to monitor current and temperature, as well as a BTMS for temperature control of the battery. This is necessary, because one of the major drawbacks of Li-ion technology is that it can only operate safely within a small operating window of between 20 and 40°C [41].

For example, it can be assumed that the service life of the battery is halved if it is operated at a temperature that is too warm for every 10K. In addition, excessive heating (>120°C) can cause the materials in the battery to decompose, which can lead to thermal runaway up to explosion. At the same time, the thermal system must also be able to provide heating power, as a battery only delivers a constant current from around +5°C [41] and should be able to be optimally conditioned despite cold ambient conditions. A typical configuration consists of a cooling circuit whose liquid is pumped to the battery packs. This is either cooled by a heat pump or heat exchanger, or heated by an electrically operated Positive Temperature Coefficient (PTC) resistor. The coolant can cool or heat the battery as required by flowing along the packs through channels in the housing. [53]

Charging processes

In order to minimise excessive degradation caused by charging the battery cells too fast, a maximum C-rate of 1.3 C should be set. Of course, the C-rate can always be set higher, but this also means accepting greater battery degradation and eventually requires more cooling. The C-rate is the ratio of the maximum current I_{max} to the battery capacity or energy storage capacity Q and therefore inversely the charge/discharge rate [42, 40]:

$$C = \frac{I_{(dis)charge}}{Q_{Bat}} \tag{3.4}$$

where $I_{(dis)charge}$ is the current applied during charging/discharging in [A] and Q_{Bat} is the capacity of the battery cell or pack in [Ah].

With this specification, the charging process (from 15...90 %) is completed in about 45 minutes, even with those small charging speeds of just 1.3C. If the battery has not been fully discharged to 15 % on the previous mission, or if the full capacity range is not required for the next mission, the charge time, and therefore the waiting time, can be reduced significantly. In addition, in the above-mentioned capacity range it is partly possible to charge in Constant Current (CC) mode, where the battery is not severely degraded when charging > 1.3 C. With

charge rates of 2C or even 5C, very fast charging in t >= 12 min is possible if required, provided the future airport's charging structure is designed for this [40, 41, 42]. Thus, with future improvements of fast charging technologies a way faster turnaround time than 45 minutes can be achieved.
An appropriate charging strategy within the airport structure is discussed in more detail later in chapter 5.1.

Service life and maintenance
With proper use (avoiding degrading mechanisms such as charging above 90 %, long storage at high SoCs and operation in undesirable temperature ranges), a battery can survive over 3000 full charge cycles in the future before reaching its End of Life (EoL), and the trend is rising [54, 40]. Since the aircraft are in frequent use, it is the charging cycles that will be the limiting factor in service life, not calendar ageing. A full charge cycle is defined here as a complete discharge and recharge in the range between the minimum and maximum permitted SoC (15 % and 85 %). This implies that shorter flight distances without a complete discharge of the specified amount of energy will reduce the service life of the battery packs to a lesser extent. Under these assumptions, approximately 3500 missions on the defined routes can be flown before the battery reaches the critical number of charge cycles. However, to ensure reliable operation, the battery pack should be replaced before reaching the specified number of cycles, once 20% of its original capacity has been lost [41]. As degradation near 20 % means that the required amount of energy can no longer be provided for the longest distances, smart route planning must also take into account that more severely degraded packs can only be used for shorter distances up to their EoL, and that a higher proportion of SAF may need to be carried to compensate for the lower amount of energy due to degradation. Since the battery packs assembled from many small cylindrical cells, it is possible to identify degraded cells or areas for targeted replacement. This has a positive impact on the aircraft costs and saves a lot of resources.

The integration of the batteries is designed to accommodate regular inspections and replacements. In the front fuselage, the battery compartment is accessible through a cargo door on the right side of the aircraft. The stacked battery packs there feature minimal connectors to enable quick removal. For batteries located in the wing, access is provided from below. The wing structure allows for the lower cover panels between each rib to be individually removed, simplifying battery maintenance procedures.
As the coolant in the cooling system needs to be changed at regular intervals, both cooling circuits are fitted with drain nozzles on the wings. This makes it easy to change the coolant.

Safety
To comply with safety requirements, the battery may not pose a risk to the aircraft, even in extreme scenarios. For this reason, the battery integration takes potential hazards emerging from the battery into account. A risk originating from the battery itself is fire. Once a battery ignites, it is difficult to extinguish. To prevent ignition, a battery pack is shut down when exceeding a temperature of 55°C, so that the current output flow stops and thermal runaway can be avoided. This mechanism occurs because from this temperature the exothermic decomposition of the solid-electrolyte-interphase passivation layer begins and the battery heats up increasingly fast until all materials decompose and thermal runaway occurs [39]. The concerned battery packs will only be restarted once they are cooled down to a safe level and no further malfunctions occur. Therefore the battery is designed in such a way that the temperature of each individual cell can be monitored. In addition, the cylindrical round cells are interconnected in small individual packs so that single cells can be quickly disconnected from the grid in an emergency, preventing a large fire from spreading in the event of a small defect [55]. In accordance with existing fire zone regulations in the *CS-25* [21], all flight critical equipment within the battery compartment and the compartment walls are designed to withstand the heat of a battery fire for at least 5 minutes.

In addition to the inherent dangers associated with the battery itself, the battery must also be protected against external hazards. In the event of a wheels-up landing or crash, the batteries located within the fuselage are at risk of crushing and scraping action that could potentially trigger a battery fire. For this reason, the fuselage structure beneath the batteries is designed to absorb crash loads. For this reason, an integral structural component incorporating energy-absorbing struts is designed in accordance with [56]. Another particular risk to be considered is the event of a propeller blade rupture. As a blade release represents a very high energy debris, the battery placement avoids being in the trajectories of potential blade releases. A final external thread for the batteries originates from fluid spills, that could hit the battery and cause short circuits. For this reason, hydraulic and SAF pipes are not located above the batteries and spill barriers are installed where pipe connections are too close to the battery.

3.6 Range Extender System

The range extender system is key to the feasibility of the *VoltAirs-95* aircraft. It is a second source of electric power for the DEP and secondary on-board systems on longer flights and during diversion. By doing so, it enables to operate more energetic efficiently on a range of missions other than the design point.

Figure 3.4 shows the integration of the RE system into the powertrain architecture. The gas turbine provides mechanical power to the generator, which converts it into electrical power. A transformer rectifier unit is used to feed the power into the 800 V bus network, that supplies the DEP motors. In order to comply with *CS-25* redundancy requirements [21], the system is of a duplex design. The maximum continuous shaft power of each gas turbine is set to 3000 kW, which is a similar power rating like a *General Electric T64* turboshaft engine [57]. The conversion efficiency of the gas turbine $\eta_{turb} = 0.33$ is established in accordance with [58], and the efficiency of the generator and rectifier $\eta_{gen} = 0.93$ with [14].

Unlike usual turbofan engines, the RE gas turbine can be operated at its ideal point of thermal efficiency at all times, which enables greater energetic efficiency. The powertrain architecture allows excess power not required for propulsion, for example during cruise, to be used to recharge the battery.

Just as an auxiliary power unit in conventional aircraft, the RE system is integrated into the rear unpressurised fuselage of the *VoltAirs-95*. To provide the gas turbines with a sufficiently large airflow, the rear fuselage is equipped with an air intakes on each side, shown in Figure 3.6. The incoming airflow is further used to cool the electrical power components of the RE. The non-ideal condition of the oncoming airflow due to the fuselage boundary layer and propeller wakes must be taken into account for the detailed intake and turbine design. The air intakes are retractable in order to avoid additional fuselage drag when the RE is not in use. The retraction system is driven by electric actuators that move the retraction struts and the inlet flap. The connection of the inlet flap to the fuselage skin is realised by a morphing foil that adjusts its shape to the current position, similar to the morphing flaps in section 3.2.

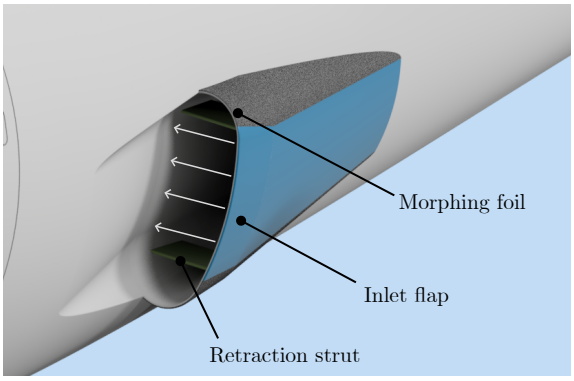

Figure 3.6: RE air intake and retraction system

Because the rigid V-tail makes it necessary to trim the aircraft by changing the CG, the SAF is stored in two separate Fuel Tank (FT)s integrated into the fuselage. As is typical of long-haul aircraft, the fuel management system handles the aircraft's trim by pumping fuel from one tank to the other [59]. For maximum momentum, the tanks are located far away from the CG, as can be seen in Figure 3.5. In order to trim out the aircraft in all loading conditions, the fuel tanks are dimensioned larger than necessary for the maximum fuel required in the 894 km mission. Due to the position of the tank, they can be subject to damage in the event of a tail strike or wheels up landing. Recent publications on the approval of the *Airbus A321XLR* suggest a structural reinforcement of the fuselage structure beneath the tanks [60].

3.7 Aircraft on-board Systems

On most conventional aircraft, the engine is the primary power source for the hydraulic system, the bleed air system, and the electrical distribution network [61]. The established propulsion architecture of the *VoltAirs-95* therefore has severe impacts on other aircraft on-board systems.

The elimination of the engine-driven hydraulic pumps motivates to do without a central hydraulic architecture. Instead, a electro-hydraulic system and Electro-Hydrostatic Actuator (EHA)s are installed. The electro-hydraulic system incorporates an Hydraulic Power Pack (HPP), which combines two electric motor-driven pumps and the hydraulic equipment into a single Line Replaceable Unit (LRU), which is installed in the belly fairing area. The HPP drives single hydraulic network, to which the landing gear, landing gear doors, one flap Power Control Unit (PCU) motor, and two V-tail actuators are connected. All other flight control surfaces are driven by EHAs, powered by the electric system, and a second PCU electric motor provides redundancy for the flap system. This architecture enables a hydraulic-free wing, reducing installation and maintenance cost [62].

Without an engine-driven bleed air system, the architectures of the Environmental Control System (ECS) and anti-ice system are similar to that of the *Boeing 787* [63]. The cabin air is in drawn in via dedicated fresh air inlets and pressurised by electrically driven compressors. Subsequently, the pressurised air is tempered with air conditioning packs, mixed with recirculated air in the mixer unit and fed into the cabin air distribution system. Furthermore, the anti-icing system is designed as an electro-thermal system. The leading edge of the aircraft wing and engine nacelle are equipped with heating blankets. The power demand of the electro-thermal system is reduced through the heat radiation of the motor power electronics located in the wing leading edge.

The increased number of electrically-powered systems increases the power rating of the secondary electrical distribution network. The various busses are powered by the 800 V bus trough transformers and static inverters. For emergency cases, a Ram Air Turbine (RAT) generator can supply electrical power to flight critical components.

4 Aircraft Technical Data

The design process of the *VoltAirs-95* is supported by aircraft dimensioning calculations. In this process, the structural mass estimation, aerodynamics, and aircraft performance are interdependent, necessitating an iterative approach. The technical data of the converged design demonstrate the feasibility of the aircraft concept.

4.1 Mass Estimation

The structural masses are mainly calculated using semi-empirical Class-II methods by Torenbeek [64]. Table 4.1 shows the OEM breakdown of the *VoltAirs-95*. For the high aspect ratio wing and V-tail, the load distributions along the wing coordinate are computed and the structures are dimensioned to withstand the calculated stress. In the load model, the six battery packs installed within the wing box counteract the aerodynamic bending loads. Furthermore, the active load alleviation system justifies a reduction of the certification load limit to 2.0 g [65], thus significantly reducing wing mass. Material properties are taken from [33], whereby the wing structure is manufactured out out of aluminium and the V-tail out of Carbon Fibre Reinforced Plastic (CFRP). The material choice is reasoned in section 5.5. The mass calculation for the aluminium fuselage is modified to account for the windowless fuselage design. Since SAF is only a small fraction of the energy storage weight, the Maximum Landing Mass (MLM) is very close to the MTOM, resulting in a slightly heavier landing gear. In order to estimate the masses of the electric powertrain components, methods from the literature are adopted [14, 58]. The plausibility of the calculated component masses was checked by a comparison with aircraft of similar dimensions [66].

Table 4.1: OEM breakdown

Component	Mass
Wing [33]	4 002 kg
Fuselage [64, 23]	3 531 kg
V-tail [33]	369 kg
Landing gear [67]	1 527 kg
Engine pods [14]	2 174 kg
Systems [67, 14]	3 328 kg
Range extender [58]	2 314 kg
Furnishing [64]	2 191 kg
Operator's items [64]	735 kg
$\sum$ **OEM**	20 171 kg

Table 4.2: Mass comparison

Mass category	*VoltAirs-95*	*DASH-8-Q400*
OEM	20 171 kg	17 885 kg
MPLM	9 025 kg	8 459 kg
SAF capacity	1 904 kg	5 318 kg
Battery	12 978 kg	-
MZFM	42 077 kg	26 308 kg
MLM	43 538 kg	28 123 kg
MTOM	43 981 kg	29 574 kg

A comparison of the mass breakdown of the *VoltAirs-95* and the reference aircraft, the *DASH-8-Q400* [9], is presented in Table 4.2. For *VoltAirs-95*, the Maximum Zero Fuel Mass (MZFM) is defined as the MTOM without SAF in the tanks. Due to larger dimensions, *VoltAirs-95*'s OEM is 2286 kg heavier than that of the the *DASH-8-Q400*. The difference in MTOM is significantly larger, amounting to 14 408 kg. This discrepancy is reasoned by the higher battery mass fraction required to achieve the battery-electric range, compared to the fuel mass fraction of the *Dash-8-Q400*.

4.2 Aerodynamics

In order to determine the aerodynamic forces, handbook methods in accordance with [18, 68, 33] were used and for determining the drag of the aircraft components, the handbook methods [18, 30] were utilised.

Lift
In order to represent the C_L-α curve, a linear increase in the lift coefficient to the critical range of α=14° is assumed, whereby the cruising flight is determined at an angle of attack of 3.5°. To accurately describe the stall behaviour of the wing across its entire span, a 2D-3D transformation is essential. However, given that the wing has a relatively small sweep of 5°, this does not hold a significant impact on the stall behaviour of the wing due to transverse flow at the wingtip and can be neglected.

$$C_{L\alpha} = \frac{2 \cdot \pi \cdot AR}{2 + \sqrt{4 + AR^2 \cdot (\frac{1}{cos(\phi_{25})^2} - Ma^2)}} \tag{4.1}$$

The V-tail contributes a minimal amount of lift, which serves to compensate for the tail-pitching moment of the wing. The resulting lift coefficient over alpha curve of *VoltAirs-95* is illustrated in Figure 4.1.

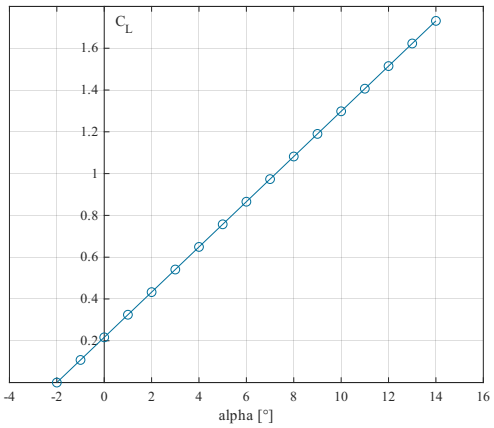

Figure 4.1: Lift coefficient vs angle of attack

The high-lift system is designed in accordance with the handbook methods set forth in [68, 33, 30].
At the maximum flap position of 40°, the maximum lift coefficient for landing is achieved, which allows to maintain a take-off field length of 1,500 metres.

Drag
Drag is the key factor in overall aircraft performance, as it influences the thrust requirements and energy consumption. One of the optimisation objectives in the design of *VoltAirs-95* is to maintain a low zero-lift drag C_{D0} by reducing the surface areas of the aircraft components. On the other hand a large the wing area is necessary for the configuration due to its high *MTOM* and short runway requirement, to achieve a realistic lift coefficient for landing. For calculating the zero-lift drag, all flows are calculated as fully turbulent, assuming that the DEP on the wing generates a turbulent wake.

The V-tail exhibits a low zero-lift drag coefficient of 0.0028, which corresponds to 13.5 % of the total zero-lift drag. By combining the horizontal and vertical stabilisers, a reduction in interference drag of approximately 5 % is achieved for the V-tail. The wing exhibits the highest zero-lift drag coefficient with 0.0066, which can be attributed to its extensive surface area. Given that the propellers are installed upstream of the wing, it is assumed that the wake is fully turbulent. For this reason, a laminar airfoil is disregarded. The nacelles constitute a significant portion of the zero-lift drag coefficient with 0.0054, which can be attributed to the utilisation of ten engines, all of which impinge upon the wing due to their upstream positioning. For the fuselage a zero-lift drag coefficient of 0.0057 is determined. The summation of all coefficients yields a zero-lift drag coefficient of 0.0206 for *VoltAirs-95*. The preceding chapter's data is incorporated to diminish the induced resistance. The drag of *VoltAirs-95* is visualised in Figure 4.3a for different angles of attack. Figure 4.3b shows the drag polar of *VoltAirs-95*.

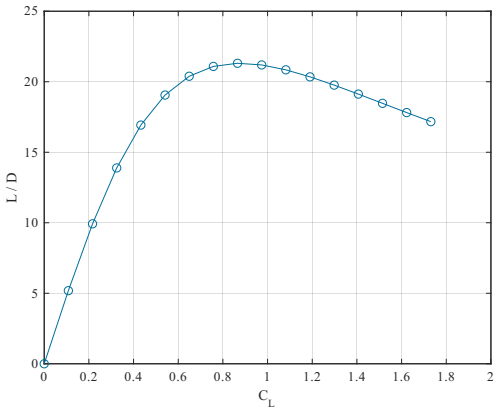

Figure 4.2: Glide ratio vs Lift coefficient

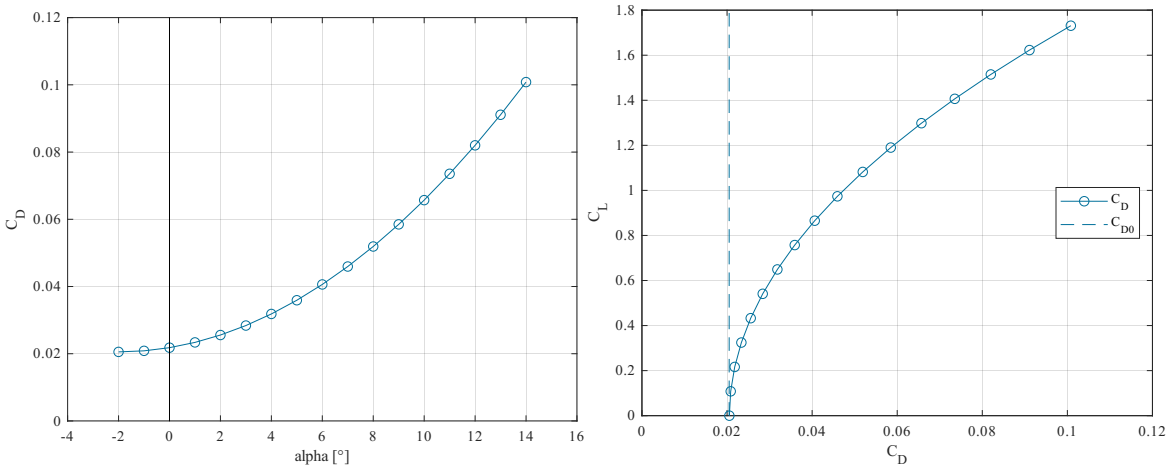

(a) Drag coefficient vs angle of attack

(b) Drag polar

Figure 4.3: Drag display

The high aspect ratio and *Oswald*-factor implies that the induced drag increases at a lower rate with the increase in angle of attack. This also permits flight with a C_{L} of 0.61 during cruise flight, resulting in a glide ratio of 20 as displayed in Figure 4.2. Nevertheless, the maximum glide ratio is realised at a lift coefficient of 0.9 and thus higher as for cruise conditions. This can be attributed to the high aspect ratio and shows also great flight characteristics in non-cruise condition. The wing loading in flight is $5174\,\mathrm{N/m^2}$.

4.3 Aircraft Performance

Flight Manoeuvring Envelope

The VN diagram for *VoltAirs-95* is shown in Figure 4.4. It is developed in line with [21, 33]. The speed values must be adapted to sea-level. The stall speed $V_{\mathrm{S1}} = 229.44\,\mathrm{km/h}$ is the intersection between the horizontal line with the load factor $n = 1$ and the curve [21]. The design manoeuvre speed V_{A} depends on V_{S1}.

$$V_A = \sqrt{2.5} \cdot V_{S1} = 362.77\,\mathrm{km/h} \tag{4.2}$$

The speed V_{A} also marks the intersection of the C_{Lmax} curve with the n_{max} line, which is valued $n_{\mathrm{max}} = 2.5$ referring to CS-25. [21] The design cruise speed V_{C} is determined with $612.72\,\mathrm{km/h}$ at cruise height and therefore must be adapted to sea-level height, which results in $424.05\,\mathrm{km/h}$. For calculating the design dive speed V_{D}, a estimation as displayed in Equation 4.3 is made in agreement with CS-25. [21]

$$V_D = 1.25 \cdot V_C = 531.28\,\mathrm{km/h} \tag{4.3}$$

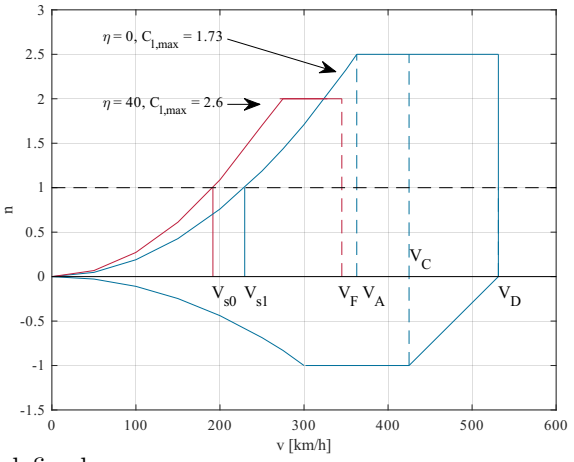

Figure 4.4: VN-diagram

Corresponding to the positive load factor, the load factor of n=-1 must be displayed in the diagram. For the curve with fully extended flaps, the stall speed V_{S0} for landing is defined.

$$V_{S0} < 1.8 \cdot V_{S1} = 191.69\,\mathrm{km/h} \tag{4.4}$$

The load factor for the flaps-out configuration is taken as n=2. [21]

Engine sizing

The electric motors are sized by evaluation of the thrust and power requirements at different operational points, such as take-off, landing and climb, taking into account failure cases, according to the CS-25 regulations [21]. For *VoltAirs-95*, a go-around procedure with One Engine Inoperative (OEI) turns out to be the critical case, with a required power per motor of 895 kW. The regular take-off with all All Engines Operative (AEO), is the next critical scenario with a power requirement of 882 kW per motor. This outcome appears logical for the hybrid design, that places an emphasis on battery power, resulting in an MLM that is just slightly lower than the MTOM. Furthermore, the landing configuration with gear and flaps fully extended creates significant drag. Notably, the AEO take-off eclipses the demand of an OEI take-off due to the lower climb angle requirement. An overview of the requirements and resulting power demands can be seen in Table 4.3. The most unfavourable environment in which MTOM operation is still within performance limits is set to the network airport of Bari (BRI) at an Outside Air Temperature (OAT) of +40°C, as it is the most likely destination for encountering hot day conditions. This is implemented in the calculations via the density altitude method [69]. *VoltAirs-95* benefits from electric engines experiencing less significant power lapse effects depending on environmental conditions [38].

Table 4.3: Critical mission scenarios, requirements and power demand

Scenario / Configuration	Minimum climb angle	Minimum airspeed	Minimum aerodynamic power per engine
Go-Around, OEI	2.7°	$1.23 \cdot V_{stall,LD}$	**895 kW**
Take-off, AEO	4°	$1.1 \cdot V_{stall,T/O}$	882 kW
Take-off, OEI	3°	$1.1 \cdot V_{stall,T/O}$	692 kW

Field performance
While take-off and go-around scenarios are covered by the power sizing, a standard landing and aborted take-off rolls require additional discussion. Traditionally, the aircraft would need to be able to come to a full stop relying only on its friction based wheel brakes. However, the combination of the high MLM and limited field length make this very challenging. After careful consideration it appears reasonable to allow for calculating the required landing field length with a higher than usual coefficient of deceleration, assuming at least partial reverse thrust can be applied in any case. This is justified by the multiple redundancies of power supply and thrust generation. Critically, unlike a conventional twin-propeller configuration, an OEI scenario does not render the reverse thrust fully inoperative for a DEP. In this case, the intact engine on the other side of the wing symmetric to the inoperative engine will automatically be set to idle after reverse thrust is selected and weight-on-wheel switches are triggered to avoid unintentional thrust asymmetry.

5 Evaluation of Operational Aspects

VoltAirs-95 is designed to hit the mark for the future demands of short-haul air travel. The operational benefits of this aircraft with regard to energy consumption, economical operation and its contribution a more sustainable aviation are discussed in the following.

5.1 Ground Operation and Recharging

As mentioned in section 2.2 the aircraft will be able to operate on regional airports, all capable of serving at least one box size “C”. In addition to the standard aircraft handling procedures for transporting aircraft, the VoltAirs-95 requires a high-performance charging system capable of supplying the maximum trip energy of 7574 kWh within the maximum charging time of 45 minutes. Due to the high current flow, the aircraft is charged with five plugs, each connecting to two battery packs. In order to mitigate the risk of arcing between the high-voltage cables, the connection ports are distributed with great separation along the aircraft. The refuelling of SAF should only commence once the battery charging process is finished. Otherwise, any SAF fumes, potentially created through improper handling, and the high-voltage chargers may pose a risk of explosion.

5.2 Mission Analysis

A major design objective of *VoltAirs-95* is to achieve a high overall energy efficiency on the given network of short-haul flights. In order to make a statement on the degree of fulfilment, a mission analysis is carried out.

The main mission is subdivided into seven segments, as shown in Figure 5.1. To calculate the required energy, the propulsive power needed in each flight condition is calculated in accordance with section 4.3 integrated over the time of the mission segment. The calculation of non propulsive power and the taxi-in and taxi-out, energy is based on assumptions made in [14]. A maximum payload of 95 passengers is assumed, and a 10 kt headwind is factored to the total flight distance to account for realistic operating conditions. The mission energy breakdown in Table 5.1 refers to the energy fuelled into the aircraft. For the battery, it is the electrical energy the aircraft is charged with, and for SAF, it is the chemical energy stored in the fuel.

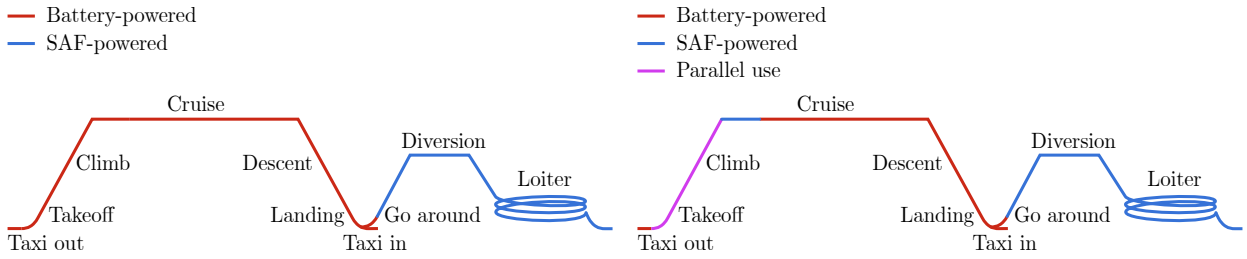

(a) Battery-electric mission (683 km) (b) Hybrid-electric missions (894 km)

Figure 5.1: Mission profiles

Two missions shown in Figure 5.1 are considered as examples. The first is the 683 km Salzburg (SZG) to Sarajevo (SJJ) , which is the longest route the *VoltAirs-95* is operating without using the range extender during the regular mission. In consequence, no mission fuel is taken on board and all of the needed propulsive and secondary energy is extracted from the battery. The mission starts with the take-off and steep 5.5° climb onto to the cruise level of 7000 m. Following a 52 minute cruise with Ma0.545, the descent starts. In order to optimise energy consumption, a continuous descent with a steep descent angle of 5.7° is flown, which allows a significant reduction in thrust. It is assumed, that ongoing automation in the air traffic control will allow such descends by EIS [70]. If no go-around is necessary, the mission ends with the approach, land and taxi out. The 7412 kWh are almost the maximum electric energy that the battery can deliver within the nominal 70 % usable SoC-range.

The second mission is the 894 km flight from Hamburg (HAM) to Edinburgh (EDI), which is the longest route the *VoltAirs-95* can fly non-stop. For hybrid-electric operation in which SAF is used during the regular mission, it is practical to burn the SAF as early as possible, as this reduces the aircraft weight and thus also the energy consumption during the rest of the flight [71]. Nonetheless, the RE is not in use during ground operation, in order to comply with the European Commission's target of zero-emission taxiing by 2050 [72]. The RE is therefore started just before take-off and contributes electric power during the take-off, climb, and early cruise segment. However, the 6000 kWh shaft power of the RE do not suffice to provide the aircraft's power demand during take-off and climb. Sizing the RE to match the peak power demands during take-off would represent an unreasonable weight increase, as the batteries can account for the power difference during these flight phases. Once the 433 kg of fuel available for the standard mission are consumed, the remainder of the flight is completed in battery electric mode. The flight profile of hybrid-electric flight is shown in Figure 5.1.
If a safe landing at the destination airport is impossible, a go-around and diversion flight is necessary. While the energy required for the diversion flight is stored in the form of SAF, it is not possible to suddenly switch on the RE in the moment of go-around, as the inlet-flaps must first open and then the gas turbines must be started. Therefore, the 548 kWh energy required for the go-around is drawn from the batteries. While this is not favourable in terms of battery service life, it does not represent a hazardous flight condition. Due to the rarity of such go-arounds, which are treated as a serious incident by operators and regulators, the reduction in battery SoC from 15 % to 9.7 % in the worst case is considered acceptable. As the second climb phase is carried out with a smaller climb angle, the required propulsive power can be fully delivered by the RE system. The remaining diversion flight including descent, loiter and landing is flown fully SAF powered, and the battery is being recharged up to 15.0 % during diversion cruise. The total amount of diversion SAF adds up to 1471 kg.
Comparing the two considered missions, it is apparent that the battery-electric 683 km mission is more energy-efficient than the hybrid-electric 894 km mission: Former has an energy consumption of 0.114 $\frac{\text{kWh}}{\text{PAX km}}$ and latter 0.150 $\frac{\text{kWh}}{\text{PAX km}}$. The reason for this difference is found in the convergence efficiency from chemically-bound SAF-energy to electric energy. While the SAF proves useful in improving the operational flexibility of the *VoltAirs-95*, it has a negative impact on the aircraft's energy consumption. This effect exacerbates when taking into account the electrical grid energy required to produce the SAF, as detailed in section 5.5.

Table 5.1: Energy consumption breakdown

	683 km mission				894 km mission			
Mission segment	Time	Propulsive power	Electric energy	SAF energy	Time	Propulsive power	Electric energy	SAF energy
Taxi out	10 min	243 kW	93 kWh	0 kWh	10 min	243 kW	93 kWh	0 kWh
Take-off	5 min	8874 kW	1006 kWh	0 kWh	5 min	8874 kW	517 kWh	1515 kWh
Climb	10 min	4617 kW	1103 kWh	0 kWh	10 min	4645 kW	101 kWh	3121 kWh
Cruise	52 min	3638 kW	4418 kWh	0 kWh	73 min	3638 kW	6067 kWh	535 kWh
Descent	10 min	400 kW	138 kWh	0 kWh	10 min	400 kW	138 kWh	0 kWh
Landing	4 min	6638 kW	607 kWh	0 kWh	4 min	6638 kW	607 kWh	0 kWh
Taxi in	10 min	243 kW	46 kWh	0 kWh	5 min	243 kW	46 kWh	0 kWh
Sum	96 min		7412 kWh	0 kWh	107 min		7569 kWh	5172 kWh

5.3 Economic Analysis

A product may be brilliantly engineered, but it can be literally worthless if it unable to fulfil its purpose in an economically viable way. To determine the economic performance of *VoltAirs-95*, DOC methods from [15] are used. The methods classify the DOC in non-recurring costs (consisting of capital and crew costs) and recurring costs (consisting of maintenance- and energy costs and fees) and calculate the cost of operating one aircraft for one year.

$$DOC = DOC_{cap} + DOC_{crew} + DOC_{MC} + DOC_{fees} + DOC_{energy} \tag{5.1}$$

The DOC of the *DHC-8-Q400* reference Aircraft, which is assumed to fuelled by 100 % SAF in 2050 can be calculated with [15] without any adaptations. However, since this method was originally developed to assess the costs of conventional kerosene powered aircraft, it must be adapted to address the specialities of battery-electric flight for the *VoltAirs-95*. In the following, the modifications made to the DOC approach are described.
The capital costs are the annual costs of the acquisition of the aircraft, consisting of the aircraft delivery price, the depreciation period and some financial parameters.

$$DOC_{cap} = p_{AC} \cdot (a + f_{ins}) \tag{5.2}$$

These parameters are taken from [15, 73], unless specified otherwise in the DLR challenge task. [15, 73] also provide the formulas for calculating these parameters. Table 5.2 summarises the parameters used.

Table 5.2: Parameters used for DOC calculation

Parameter	Value	Unit
Insurance rate	5.00%	-
Residual Value factor	5%	-
Interest Rate	5%	
Depreciation Period	20	years
Annuity factor	7.87305%	-
Profit Margin per Aircraft	20%	-
Miscellaneous factor	20%	-
Labour Rate	\$50.00	\$/h
Cost Burden	2	-
Range dependent ATC factor	1	-
Handling fees	\$0.10	\$/kg
Landing fees	\$0.01	\$/kg
Assigned price for electric energy	0.038	\$/kWh
Assigned price for SAF	0.104	\$/kWh

The aircraft delivery price is based on the price of the aircraft RC_{elec}, the proportion of the development costs NRC and some other financial parameters based on [73].

$$p_{AC} = \left(RC_{elec} + \frac{NRC}{n_{AC}} \right) \cdot (1 + PM_{AC} + f_{misc}) \tag{5.3}$$

For a first estimate the development costs were set to 800 mioUSD and the number of aircraft sold is estimated at 2500. The development cost are assumed roughly twice the cost of the *DHC-8-Q400* [74], taken into account the new technologies implemented in the aircraft. 2500 aircraft is the combined number of sold Dash-8 and ATR-72, assuming that the *VoltAirs-95* can substitutes of the market. The costs of the aircraft are calculated via the approach from [73] with the modifications mentioned in the task, consisting of the price for a reference kerosene-powered aircraft and the additional costs of the battery. The battery price was given with 200 \$/kWh. One aircraft requires the aquisition of multiple batteries, given that it must be changed after it reaches 80 % of its original capacity. At this point the battery is not worthless, but can be resold for a second life. Assuming the 200 \$/kWh original price and resale values found in the literature [75, 76], the effective battery costs is assumed to 100 \$/kWh.

$$RC_{\text{elec}} = RC_{\text{kerosene}} + n_{\text{battery}} \cdot p_{\text{battery}} \tag{5.4}$$

The costs of the reference aircraft are calculated via the mass-estimation method from [15]. The masses of *VoltAirs-95* and the battery capacity are adopted from section 4.1. The number of batteries n_{battery} is based on the possible cycles of the batteries, described in section 3.5. Hence, each *VoltAirs-95* aircraft will use ten batteries within in the depreciation period.
The crew costs consist of the number of crews necessary to operate the aircraft through the year CC, the average salary for flight crew and flight attendants and the number of flight attendants. (One for every 50 PAX).

$$DOC_{\text{crew}} = CC \cdot (S_{\text{FA}} \cdot n_{\text{FA}} + S_{\text{FA}}) \tag{5.5}$$

The maintenance costs are divided into the material costs of the airframe, the labour costs of the airframe maintenance and the maintenance costs of the engines. Since only minor improvements on the airframe were made, its maintenance costs do not need to be modified. The maintenance cost of the engine can be subdivided into the maintenance cost of the electric powertrain and the maintenance cost of the SAF-powertrain.

$$DOC_{MC} = MC_{\text{AF,MAT}} + MC_{\text{AF,Labour}} + MC_{\text{E-Power}} + MC_{\text{SAF-Power}} \cdot f_{SAF} \tag{5.6}$$

[48, 77] find, that the maintenance cost of the electric powertrain can be estimated by 75% of the maintenance cost of a conventional powertrain. The Maintenance Cost (MC) of the SAF powertrain can be calculated with conventional formulas, with respect to the occasional usage. Thus, this costs are multiplied by the share of flights with SAF, assuming that deterioration is mainly caused by the cycles and not the operating hours of the engine.
The fees consist of charges for air traffic control and charges for airport services, in particular the landing and ground handling fees. The first two are usually calculated as a function of the MTOM of the aircraft, giving huge disadvantage for battery electric aircraft. Hence, [73] claims that it would be unreasonable for policymakers to not change these charges, so for an appropriate comparison the fees of the kerosene reference aircraft shall be used. However, the handling fee depends on the payload, hence no changes need to be made here.

$$DOC_{\text{fees}} = DOC_{\text{fees,ATC}} + DOC_{\text{fees,AP}} \tag{5.7}$$

The energy costs are calculated based on the reference mission described in section 2.3. The prices for SAF and electric energy are given from the DLR Challenge task.

$$DOC_{\text{energy}} = p_{\text{SAF}} \cdot n_{\text{SAF}} + p_{\text{elec}} \cdot n_{\text{elec}} \tag{5.8}$$

The DOC of the *VoltAirs-95* can then be calculated. The results are presented in Table 5.3. Furthermore, the analysis of the routes in section 2.3 shows that a total of 7 *VoltAirs-95* are needed to operate the given network. With a total of 726 620 934.3 travellers per year in the network, the DOC per PAX can be calculated. A detailed discussion of the individual operating cost factors follows in section 5.4.

Table 5.3: Summary of the DOC of the *VoltAirs-95*

Type of Cost	Value
Capital costs	$ 6,036,265.88
Crew Costs	$ 2,350,000.00
Maintenance Costs	$ 1,897,309.66
Sum of the fees	$ 3,183,103.91
Energy cost	$ 525,057.23
Direct Operating Costs	$ 13,991,736.67
required A/C for the Network	7
Direct Operating Costs per Passenger	$ 0.1433/PAX

5.4 Comparison to Reference Aircraft

Finally, the performance of the *VoltAirs-95* aircraft is compared to that of the reference aircraft. The reference aircraft is chosen in a selection process, comparing the short-haul aircraft and their specifications mentioned in section 2.1 to the specification of the *VoltAirs-95*. For each aircraft, the deviations from all specification are calculated and averaged to produce a score. The Dash-8 scored the highest with 74.2 % conformance and was therefore selected as the reference aircraft. The *DASH-8-Q400* and *VoltAirs-95* aircraft are evaluated in terms of the design objectives, which are relative energy consumption and DOC.
In the comparison, it is important to note the difference in the network operations of both aircraft. This is due to the different payload-range characteristics, that is displayed in Figure 5.2.

The *DASH-8-Q400* shows a typical payload-range behaviour [78], that allows for an operational flexibility between the range of maximum payload and the range of full fuel tanks. Contrary, the battery and SAF tanks of the *VoltAirs-95* are sized to just operate the 894 km mission with maximum payload of 95 passengers, and any slight increase in range comes at the cost of a drastic decrease in available payload. As a consequence, the *DASH-8-Q400* is able to operate the whole network without the need for stopovers, while the *VoltAirs-95* needs to incorporate a stopover on 24 out of the 104 legs.

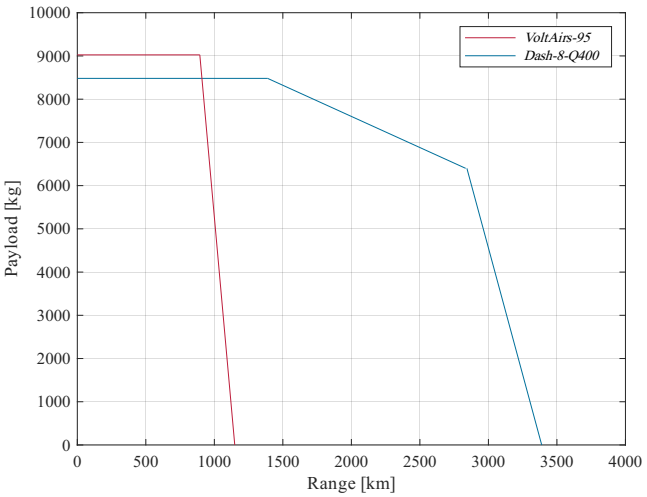

Figure 5.2: Payload-range comparison

To compare the energetic performance of both aircraft, the mission energy for each route within the network is estimated, taking into account the related occupancy rate of the aircraft. Due to a lack of detailed aircraft performance data available for the *DASH-8-Q400*, a detailed mission analysis as in section 5.2 cannot be performed. Instead, the fuel consumption is estimated with a simplified BREGUET mission including a lost range for take-off and [19]. The necessary performance data is reverse calculated with [9]. To allow for a fair comparison between both aircraft, the mission energy of the *VoltAirs-95* is calculated with the same approach, however this simplification increases the energy consumption by ca. 8 % compared to the detailed mission analysis. Figure 5.3 shows the comparison of the energy consumption per passenger kilometre. While the improvement varies per route, it is clear that the *VoltAirs-95* achieves significantly better energetic performance compared to the *DASH-8-Q400*, even on the routes with stopover. The overall energy consumption for the whole network is reduced from 0.246 $\frac{\text{kWh}}{\text{PAX km}}$ to 0.136 $\frac{\text{kWh}}{\text{PAX km}}$.

A comparison of the total and relative share of the individual cost factors of the *DHC-8.Q400* and the *VoltAirs-95* reveals various similarities and differences. The biggest difference is undoubtedly the capital costs, as these make up almost half of the DOC for *VoltAirs-95*. This is due to the high cost of the battery and in particular the fact that it has to be replaced after 3500 cycles. Therefore, in total ten batteries are required to operate the for the assumed service life of 20 years. The other major difference is the energy costs. This is mainly due to the high price of SAF and the *DHC-8.Q400*'s higher fuel consumption, allowing significant savings in the mission energy cost.

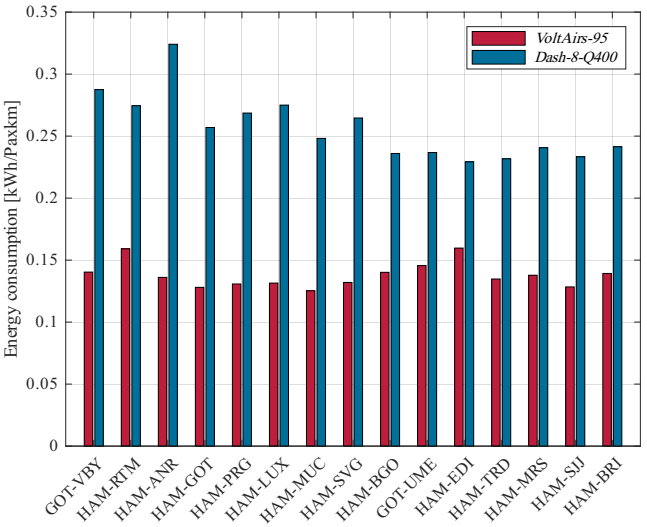

Figure 5.3: Comparison of energy consumption

The slightly higher maintenance costs for *VoltAirs-95* are caused by the sophisticated powertrain. Although, the electric components require less maintenance than conventional engines and the range extender is only used occasionally. The fees for the *DHC-8-Q400* are higher, because the aircraft needs more flights to transport the same amount of passengers due to the smaller cabin. Due to the higher cruise speed, this has no impact on the required number of aircraft, but the fees for the additional flights need to be payed. Last but not least, the crew cost are equal because both aircraft need the same flight crew and number of flight attendants. In total, the DOC of the *VoltAirs-95* is 9.17 % higher than the DOC of the SAF-powered *DHC-8-Q400*. This is not so much that the aircraft would be considered uneconomical. With further adjustments by the policy makers, for example a fee schedule that takes into account the energy consumption or aircraft emissions of the aircraft, the *VoltAirs-95* is even more competitive. Otherwise, if the SAF-price would be higher than expected (due to supply shortages, competing applications, or policies subsidising alternative propulsion concepts), the *VoltAirs-95* could even get an advantage in DOC. The break-even point for equal DOC on both concepts is a SAF-price of 0.1457 \$/kWh (1.7487 \$/kg) which is a rise of 40.1 % of the SAF-price given in the task.

5.5 Life Cycle Assessment and Emissions

In the context of the world's march towards a circular economy [79], as part of the United Nations (UN) Sustainable Development Goals (SDG) [80], it is indispensable to not only produce an efficient aircraft in operation, but to also consider its whole life cycle and assess its environmental impact. The aim is to develop a solution that is sustainable and resource efficient throughout the different life cycle phases. This is not just limited to the type and amount of energy used, but also to the waste products in terms of their recyclability. Although a full Life Cycle Assessment (LCA) over the entire service of the aircraft is not possible during the conceptual design phase, key points are discussed in this section.

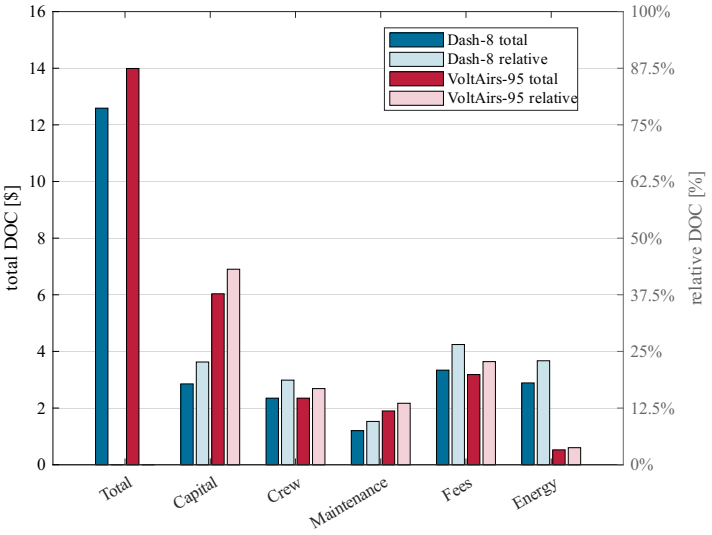

Figure 5.4: Comparison of the DOC elements

Battery impact

In the production of the aircraft, the amount of energy required to manufacture the batteries has a particularly large impact on the resources required. The production of each 100 kWh NMC lithium-ion battery currently requires 85.5 kg of nickel, 9.7 kg of manganese, 11.1 kg of cobalt and 9.2 kg of lithium as well as 37.9 kg of aluminium and 73.9 kg of copper as raw materials, when no recycled materials are included [40].
Assuming that only sustainable green electricity is used for battery plants in the future, the production itself will be carbon neutral. However, it should also be noted that battery production requires energy and other resources not only at the production site itself, but also during the extraction and transport of the raw materials (e.g. by ship, train, etc.) and may thus also generate Greenhouse Gas (GHG) emissions. The main advantage of using a battery to power the aircraft is that there are no local emissions and, if the aircraft is powered by green electricity, there are no emissions from the production of the electricity either. This means that in aircraft operation there will be no more emissions (during battery-electric operation) and thus the GHG emitted during production can be amortised over its lifetime (see also Figure 5.5). Nevertheless, it is important to increase the efficiency of the entire value chain and to achieve a high rate of recycled battery materials at the end of the product cycle, as the production of new batteries from raw materials has a significant impact on the environment. It is known from the automotive sector that it is already technically possible to recycle the metals from lithium-ion batteries with high efficiency. As high recycling rates for electric car batteries have already been set for 2030, it can be assumed that each of the aircraft batteries used can and must be largely recycled. [40]
Since the battery needs to be replaced after 3500 charge/discharge cycles (or 20% degradation) due to high safety requirements as explained in section 3.5, there are two strategies to improve the ecological footprint at this point. The first is the detection of individual damaged cells or areas, which can allow a targeted replacement. Furthermore, when a whole battery reaches its EoL, it should not be discarded but rather sold for further use in stationary applications. Only when the cycle or degradation standards can no longer be met for the secondary application after many more hours of use, the battery will be recycled. This not only improves the environmental footprint of the *VoltAirs-95* by producing less waste and using less energy overall, but also provides a significant DOC benefit through battery resale.

Impact of airframe material

The majority of *VoltAirs-95*'s airframe structure is made from aluminium alloys. The material's design choice of aluminium alloys over CFRP is mainly driven by LCA considerations. First, the manufacturing of aluminium structures for aircraft is well developed and optimised. Aluminium production, deformation, machining, and tempering have proven to be significantly less energy intensive than the production of CFRP structures [81]. In service, aluminium airframe structures benefit from a good maintainability, being easily repairable. Furthermore the aluminium airframe structure can be dismantled and the material recycled, when the aircraft reaches

its EoL. Secondary aluminium production reduces energy demand by 95 % compared to primary aluminium production [82], demonstrating the significant value of airframe recycling to the overall environmental footprint. These advantages are graded stronger than the increase of in-flight energy demand due to heavier structures compared to a CFRP airframe.

Comparison of the Global Warming Potential of VoltAirs-95 with the reference aircraft

Calculation of Global Warming Potential (GWP) is a LCA method that describes the global warming impact of a tonne of GHG relative to a tonne of CO_2 emitted over 100 years. To make it easier to compare the impact of different exhaust gases on the environment, the amount of exhaust gas is converted into CO_2 equivalents. Thus, e.g. a gas that would be four times as harmful as CO_2, would receive a factor of four. Based on Hauschild et al. [83], the exhaust gases i emitted for the flight mission can be calculated as follows:

$$GWP_i = \sum(x_i \cdot c_i) \tag{5.9}$$

where x_i is the quantity of GHG i emitted per defined distance in [kg] and c_i is the CO_2-equivalents of the GHG i in [t CO_2-eq./t_i]

The CO_2-equivalents of the substance i, c_i, can be calculated with:

$$c_i = h_{U,i} \cdot c_i^{spez} \tag{5.10}$$

where $h_{U,i}$ is the lower heating value of the fuel used in [MJ/kg_i] and c_i^{spez} is the specific CO_2-equivalent related to the amount of the fuel energy in [kg CO_2-eq./MJ_i].

For every tonne of kerosene used, 3.16 tonnes of CO_2 are emitted [84]. This roughly corresponds to the typical values for SAF of up to 70 g_{CO_2}/MJ_{SAF} for Hydroprocessed Esters and Fatty Acids (HEFA) [14, 85] with a lower heating value of $h_{U,SAF} = 43.2171$ MJ/kg. When using algae values as low as 1.5 g_{CO_2}/MJ_{fuel} or even negative values are possible [85]. However, as this is not yet state of the art, the following calculation is based on the assumption that $c_{SAF} = 3$ t CO_2-eq./t_{SAF}. The following Table 5.4 compares the CO_2 equivalent emissions of the SAF-powered *Dash-8-Q400* reference aircraft and the *VoltAirs-95* aircraft for the shortest route in the specified network and the longest route possible without stopover for the *VoltAirs-95*.

Table 5.4: Comparison of CO_2-equivalents generated during defined flight missions with the reference aircraft *Dash-8-Q400* and the *VoltAirs-95*

		Dash-8-Q400		*VoltAirs-95*		
	Range [km]	m_{SAF} [kg]	GHG emissions [$tCO_2 - eq./range$]	E_{Bat} [kWh]	m_{SAF} [kg]	GHG emissions [$tCO_2 - eq./range$]
shortest route	361	653	2.064	7795	0	0
longest route without stop	894	1399	4.421	7569	433	1.377
longest route without stop, adjusted	894	1399	0.882	7569	433	0.2754

As SAF is made from biomass that has already stored CO_2 during its lifetime, the carbon cycle is closed and the environmental footprint can be expected to be up to 80% better than kerosene made from oil stored below the earth's surface. Based on this assumption, an adjusted net CO_2 emission of 20% of the original CO_2 equivalent c_i can be calculated. [86, 87, 88]

As expected, the *VoltAirs-95* produces no emissions on the shortest battery flight of 361 km, whereas the reference aircraft would produce 2.064 tonnes of CO_2 equivalents on the same flight. The *VoltAirs-95* is also superior to the Dash-8-Q400 when using the SAF operated RE for short periods, as the majority of the trip is still done on battery power. Thus, the aircraft developed results in 69 % less CO_2-equivalent emissions on the longest non-stop flight.

The batteries implemented in the *VoltAirs-95* create between 35 and 87.5 kg CO_2-eq./$kWh_{capacity}$ during production phase [58, 54] (see possible range marked in Figure 5.5), but when charged with purely green electricity they operate carbon neutral during use phase. Compared to the SAF-powered reference aircraft, this is a good

indication of the number of miles it takes for the battery to amortise its production emissions (see Figure 5.5). Under these assumptions, the CO_2 emissions associated with battery production pay for themselves after a range of approximately 87,366 km, but no more than 212,175 km, compared to a full SAF-powered aircraft. This would mean less than 250 flights for the shortest all-electric flight in the route network under consideration, before the battery packs pay for themselves in environmental terms.
Thus, the above considerations show that the designed aircraft can have much better GWP values than the SAF-powered *Dash-8-Q400*, without even taking into account the fact that CO_2 and all other types of emissions have a greater impact on global warming at high altitudes than at ground level. If this was taken into account, the *VoltAirs-95* would be even more sustainable, because every kilometre flown at high altitude with electric power and no emissions would be even more sustainable.

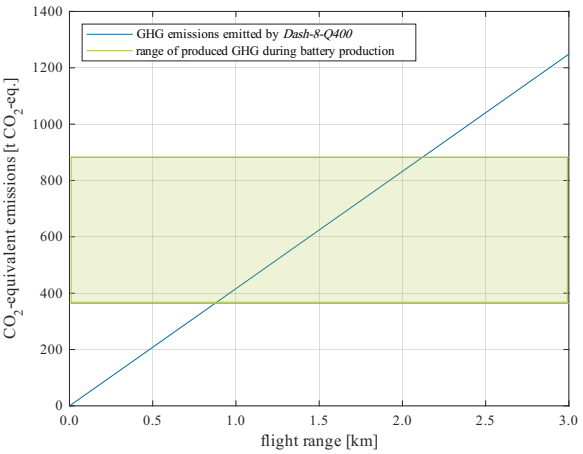

Figure 5.5: CO_2-equivalents caused by a certain range with kerosene compared to using batteries

Further theoretical considerations on the fuel cycle

Although this consideration should not have a direct impact on the LCA calculations, as the system boundary excludes fuel production, it did influence the decision for developing a predominantly electric aircraft. This choice is due to the greater environmental impact associated with production of SAF compared to electricity as described following:

1. A significant amount of energy is required for SAF propulsion to cover relatively short distances, as the conversion efficiency to electricity in the RE is around $\eta_{RE} = 40\,\%$, whereas batteries have only minimal discharging and conversion losses, with $\eta_{bat} = 90\,\%$. [14]

2. The production of SAF requires a significant amount of primary energy due to higher losses and more conversion steps for generation and transport compared to the production of electrical energy. According to DeVries et al.[14], power-to-liquid SAF production requires 5-9 kWh of primary energy for every 1 kWh of drive energy due to various conversion losses (compare Figure 5.6a). In contrast, battery-powered systems are much more efficient in converting and utilising energy with consuming only 1.3 kWh primary energy per 1 kWh drive energy during grid-to-tank and tank-to-shaft procedures (see Figure 5.6b).

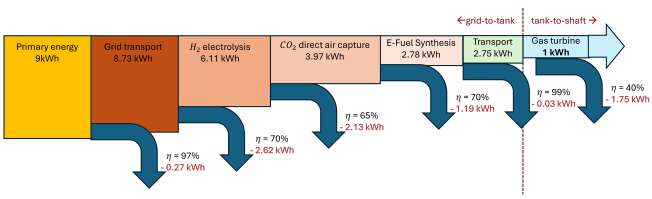

(a) Sankey diagram of energy required for shaft electricity production with SAF propulsion

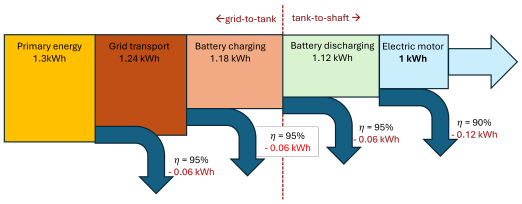

(b) Sankey diagram of energy required for shaft electricity production with battery storage

Figure 5.6: Sankey diagrams of losses during shaft electricity production based on [17]

6 Research Roadmap and Future Development

The TRL is a common metric for characterising a technologies stage of development and ease of application. To provide a perspective on the feasibility of *VoltAirs-95*, Table 6.1 displays the TRL of its key technologies. The aircraft is designed with a wide variety of potential and expected technological improvements over its service life in mind, that will increase the range or transport capability over time. The following list presents improvements and modifications considered:

Key technology	TRL	Source
Windowless fuselage	9	[89]
Li-ion batteries	8	[39]
High power electric motor	5	[90, 36]
DEP	4	[38]
Morphing wing	8	[91]

Table 6.1: TRL of key technologies

1. **Short haul mass reduction:** By removing battery packs not required for exclusive short-haul operation, take off mass is reduced allowing for lower energy consumption and airport fee reduction.
2. **Battery technology:** As battery technology continuously improves, longer battery life and higher energy densities reduce the amount of required battery replacements and enable operating longer routes with an otherwise unchanged aircraft configuration (constant MZFM).
3. **Aircraft family concept:** With higher performing batteries, cabin size and battery capacity can be increased to optimise DOC and energy efficiency for different ranges and PAX demand.
4. **Advanced aerodynamics:** Introduction of foldable wingtip propellers results in a reduction of induced drag while maintaining the permitted airport box size.

7 Conclusion

VoltAirs-95 addresses the problem statement of the DLR Design Challenge 2024 in a cautious and considered manner. After a comprehensive and methodical examination of the design task, considering a wide range of potential solutions, we determined *VoltAirs-95* to be the optimal configuration for the constrained design space possessed by the given requirements. The design focuses especially on an appropriate balance between feasibility and the degree of innovation employed. While prioritising energy efficiency and environmental impact, the concept also incorporates improved noise characteristics, reduced total life cycle impact, and a new passenger experience.
VoltAirs-95 features game-changing improvements in energy efficiency of 55 % per passenger kilometre. The drastically reduced environmental impact extends beyond the scope of operational CO_2 emissions (-94 %), encompassing life cycle considerations. Notably, economic viability is retained with only a moderate 9 % increase of DOC. Incorporating potential improvements and modifications from the beginning of the design process ensures that the aircraft will remain competitive for decades to come upon its entry into service in 2050. In summary, the VoltAirs-95 represents a realistic scenario for the regional air transport of the future that fulfils the requirements of the DLR Design Challenge 2024 in a sustainable and cost-efficient manner.

A References

[1] European Comission. *Consequences of climate Change*. URL: https://climate.ec.europa.eu/climate-change/consequences-climate-change_en.

[2] Klöwer, M. et al. "Quantifying aviation's contribution to global warming". In: *Environmental Research Letters* 16.10 (2021), p. 104027. DOI: 10.1088/1748-9326/ac286e.

[3] International Air Transport Association. *Resolution on the Industry's Commitment to reach Net Zero Carbon Emissions by 2050*. Boston, USA, 2021.

[4] International Civil Aviation Organisation. *Resolution A41-21: Consolidated statement of continuing ICAO policies and practices related to environmental protection - Climate change.* Montreal, Canada, 2022.

[5] Air Transport Action Group. *Waypoint 2050*. 2021.

[6] Embraer. *Embraer E190 Specifications*. URL: https://www.embraercommercialaviation.com/wp-content/uploads/2017/02/Embraer_spec_190_web.pdf.

[7] Bombardier. *CRJ Series*. URL: https://www.mhirj.com/themes/bca/pdf/Bombardier_CRJ_Series_Brochure.pdf.

[8] ATR-Aircraft. *ATR 72-600*. URL: https://www.atr-aircraft.com/aircraft-services/aircraft-family/atr-72-600/.

[9] De Havilland Aircraft of Canada. *Dash 8-400 Spec Sheet*. 2022.

[10] Fokker. *Information Booklet Fokker 100*. URL: https://www.fokkerservicesgroup.com/media/emccsdnm/fsg_fokker-100.pdf.

[11] Verein deutscher Ingenieure. *VDI 2221-1*.

[12] ICAO. "Annex-14". In: (1951).

[13] IFATC. *Airport database*. URL: https://ifatc.org/airports (visited on 07/21/2024).

[14] DeVries, R. et al. "A New Perspective on Battery-Electric Aviation, Part II: Conceptual Design of a 90-Seater". In: *AIAA SCITECH 2024 Forum*. Reston, Virginia: American Institute of Aeronautics and Astronautics, 2024. ISBN: 978-1-62410-711-5. DOI: 10.2514/6.2024-1490.

[15] J. Thorbeck with remarks by D. Scholz. "TU Berlin DOC Method". In: (2013).

[16] Staack, I.; Sobron, A., and Krus, P. "The potential of full-electric aircraft for civil transportation: from the Breguet range equation to operational aspects". In: *CEAS Aeronautical Journal* 12.4 (2021), pp. 803–819. ISSN: 1869-5582. DOI: 10.1007/s13272-021-00530-w.

[17] DeVries, R.; Hoogreef, M. F. M., and Vos, R. "Range Equation for Hybrid-Electric Aircraft with Constant Power Split". In: *Journal of Aircraft* 57.3 (2020), pp. 552–557. DOI: 10.2514/1.C035734.

[18] Torenbeek, E. *Advanced aircraft design: Conceptual design, analysis, and optimization of subsonic civil airplanes*. Aerospace series. Chichester, West Sussex, United Kingdom: John Wiley & Sons Inc, 2013. ISBN: 978-1-118-56811-8. DOI: 10.1002/9781118568101.

[19] Torenbeek, E. "Cruise Performance and Range Prediction Reconsidered". In: *Progress in Aerospace Sciences* 1997.33 (), pp. 285–321. ISSN: 03760421. DOI: 10.1016/S0376-0421(96)00007-3.

[20] Code of Federal Regulations. *14 CFR 91.533*. URL: https://www.ecfr.gov/current/title-14/chapter-I/subchapter-F/part-91/subpart-F/section-91.533 (visited on 07/21/2024).

[21] *CS-25 Amendment 28*.

[22] Bagassi, S.; Lucchi, F., and Persiani, F. "Aircraft preliminary design: a windowless concept". In: *5th CEAS 2015 Proceedings* (2015).

[23] Moruzzi, M. C. and Bagassi, S. "Preliminary design of a short-medium range windowless aircraft". In: *International Journal on Interactive Design and Manufacturing (IJIDeM)* 14.3 (2020), pp. 823–832. ISSN: 1955-2513. DOI: 10.1007/s12008-020-00676-7.

[24] Misol, M., ed. *Experiments on noise reduction in aircraft with active sidewall panels*.

[25] Ira H. Abbott, Albert E. von Doenhoff, Louis S. Stivers Jr., ed. *Wartime Report: Summary of Airfoil Data*. 1945.

[26] SCHOLZ, D. "Definition and Discussion of the Intrinsic Efficiency of Winglets". In: (2018). DOI: 10.13111/2066-8201.2018.10.1.

[27] Weick, F. E. and Platt, R. C. "Wind-Tunnel Tests On Model Wing With Fowler Flap And Specially Developed Leading-Edge Slot". In: Technical Note No. 459 (1933).

[28] Hutcheson, F.; Brooks, T., and Humphreys, W. "Noise Radiation from a Continuous Mold-Line Link Flap Configuration". In: *14th AIAA/CEAS Aeroacoustics Conference (29th AIAA Aeroacoustics Conference)*. Reston, Virigina: American Institute of Aeronautics and Astronautics, 2008. ISBN: 978-1-60086-983-9. DOI: 10.2514/6.2008-2966.

[29] Sreekantamurthy, T. et al. "Elastomeric Structural Attachment Concepts for Aircraft Flap Noise Reduction - Challenges and Approaches to Hyperelastic Structural Modeling and Analysis". In: ().

[30] Dr. Jan Roskam. *Airplane Design: Part VI: Preliminary Calculation of Aerodynamic, Thrust and Power Characteristics*. 2nd ed. Lawrence, Kansas: DARcorperation, 1987.

[31] Rossow, C.-C.; Wolf, K., and Horst, P., eds. *Handbuch der Luftfahrzeugtechnik*. [Elektronische Ressource]. Hanser eLibrary. München: Hanser Verlag, 2014. DOI: 10.3139/9783446436046.

[32] Vechtel, D. and Buch, J.-P. "Aspects of yaw control design of an aircraft with distributed electric propulsion". In: *CEAS aeronautical journal* 13.4 (2022), pp. 847–860. DOI: 10.1007/s13272-022-00595-1.

[33] Heinze, W. *Entwerfen von Verkehrsflugzeugen II: Vorlesungsmanuskript*. 2024.

[34] Khalil, A. and Fezans, N. "Performance Enhancement of Gust Load Alleviation Systems for Flexible Aircraft using H ∞ Optimal Control with Preview". In: *AIAA Scitech 2019 Forum*. Reston, Virginia: American Institute of Aeronautics and Astronautics, 2019. ISBN: 978-1-62410-578-4. DOI: 10.2514/6.2019-0822.

[35] QualityWings Simulations. "Ultimate 787 Collection: Users Manual". In: Rev: V1.4.0 (2021).

[36] Andersen, H. et al. "Design and Manufacturing o fa High-Specific-Power Electric Machine for Aircraft Propulsion". In: *AIAA Aviation Forum*. Vol. 2023.

[37] Kim, H. D.; Perry, A. T., and Ansell, P. J. "A Review of Distributed Electric Propulsion Concepts for Air Vehicle Technology". In: *2018 AIAA/IEEE Electric Aircraft Technologies Symposium*. Reston, Virginia: American Institute of Aeronautics and Astronautics, 2018. ISBN: 978-1-62410-572-2. DOI: 10.2514/6.2018-4998.

[38] Moore, Mark D. "PowerPoint Presentation". In: ().

[39] Sterner, M. and Stadler, I. *Energiespeicher - Bedarf, Technologien, Integration*. Berlin, Heidelberg: Springer Berlin Heidelberg, 2014. ISBN: 978-3-642-37379-4. DOI: 10.1007/978-3-642-37380-0.

[40] Kampker, A. and Heimes, H. H. *Elektromobilität: Grundlagen einer Fortschrittstechnologie*. Berlin, Heidelberg: Springer Berlin Heidelberg, 2024. ISBN: 978-3-662-65811-6. DOI: 10.1007/978-3-662-65812-3.

[41] Korthauer, R. *Handbuch Lithium-Ionen-Batterien*. Berlin, Heidelberg: Springer Berlin Heidelberg, 2013. ISBN: 978-3-642-30652-5. DOI: 10.1007/978-3-642-30653-2.

[42] Kurzweil, P. and Dietlmeier, O. K. *Elektrochemische Speicher: Superkondensatoren, Batterien, Elektrolyse-Wasserstoff, Rechtliche Rahmenbedingungen*. Wiesbaden: Springer Fachmedien Wiesbaden, 2018. ISBN: 978-3-658-21828-7. DOI: 10.1007/978-3-658-21829-4.

[43] Kawamura, H. et al. "Frontier Technology Issues: Lithium-ion batteries: a pillar for a fossil fuel-free economy?" In: (). URL: https://www.un.org/development/desa/dpad/wp-content/uploads/sites/45/publication/FTI_July2021.pdf (visited on 07/19/2024).

[44] McKinsey & Company. "Battery 2030: Resilient, sustainable and circular: Battery demand is growing—and so is the need for better solutions along the value chain." In: (). URL: https://www.globalbattery.org/media/publications/battery-2030-resilient-sustainable-and-circular.pdf.

[45] Quilty, C. D. et al. "Impact of Charge Voltage on Factors Influencing Capacity Fade in Layered NMC622: Multimodal X-ray and Electrochemical Characterization". In: *ACS applied materials & interfaces* 13.43 (2021), pp. 50920–50935. DOI: 10.1021/acsami.1c14272.

[46] Fraunhofer ISI. "Energiespeicher-Roadmap_Update 2017: Hochenergie-Batterien 2030+ und Perspektiven zukünftiger Batterietechnologien". In: (). URL: https://www.isi.fraunhofer.de/content/dam/isi/dokumente/cct/lib/Energiespeicher-Roadmap-Dezember-2017.pdf.

[47] Frühbeis, A. et al. *The "eRay" Aircraft Concept*. 2019. DOI: 10.25967/480345.

[48] Scholz, A. E.; Trifonov, D., and Hornung, M. "Environmental life cycle assessment and operating cost analysis of a conceptual battery hybrid-electric transport aircraft". In: *CEAS Aeronautical Journal* 13.1 (2022), pp. 215–235. ISSN: 1869-5582. DOI: 10.1007/s13272-021-00556-0.

[49] Auto Bild. *Porsche Taycan: Thermomanagement des E-Antriebs: Das macht den Porsche Taycan zum Beschleunigungs-König*. URL: https://www.autobild.de/artikel/porsche-taycan-thermomanagement-des-e-antriebs-18425201.html.

[50] Nigel. *Tesla 4680 Cell*. 2022. URL: https://www.batterydesign.net/tesla-4680-cell/.

[51] motor.com. *Elektroauto-Batterien: Starke Verbesserung bei der Energiedichte: Energieinhalt in kWh pro Liter hat sich seit 2008 vervielfacht*. URL: https://insideevs.de/news/582716/elektroauto-batterien-volumetrische-energiedichte-verbesserungen/ (visited on 06/16/2024).

[52] Rob McDonald. *Batteries are not Fuel*. 2023. URL: https://engrxiv.org/preprint/view/2803/5221.

[53] Wendland, R. "Ein Beitrag zur thermischen Auslegung von Fahrzeug-Batteriesystemen". PhD thesis. Technische Universität Braunschweig. DOI: 10.24355/dbbs.084-202106241143-0.

[54] Auto Bild. *E-Auto-Akku: Das muss man über E-Auto Batterien wissen: So spendet der Akku einem E-Auto die nötige Antriebsenergie*. URL: https://www.autobild.de/artikel/e-auto-akku-elektroauto-batterie-16202315.html.

[55] Bardehle, P. *Grünes Fliegen - Reisen in der Zukunft*. URL: https://www.arte.tv/de/videos/114309-000-A/gruenes-fliegen-reisen-in-der-zukunft/ (visited on 06/30/2024).

[56] Westphal, P. et al. "Structural Component with Rib and Cross Member Element". WO/2009/003870.

[57] GE Aviation. *T64 turboshaft/turboprop engines*. URL: https://www.geaerospace.com/sites/default/files/datasheet-T64_1.pdf.

[58] Wolleswinkel, R. E. et al. "A New Perspective on Battery-Electric Aviation, Part I: Reassessment of Achievable Range". In: DOI: 10.2514/6.2024-1489.

[59] Weiner, M. *Tank systems in aircraft: More than just containers*. 2023. URL: https://aeroreport.de/en/good-to-know/tank-systems-in-aircraft-more-than-just-containers#.

[60] Steinke, S. *A321XLR-Rumpfverkleidung erhält tragende Funktion*. 2024. URL: https://www.flugrevue.de/zivil/twin-erreicht-die-zielgerade-vor-der-zulassung-a321xlr-rumpfverkleidung-erhaelt-tragende-funktion/.

[61] Moir, I. *Aircraft Systems: Mechanical, Electrical and Avionics Subsystems Integration*. 3rd ed. Vol. v.52. Aerospace series. New York: John Wiley & Sons Incorporated, 2008. ISBN: 978-0-470-05996-8.

[62] Trochelmann, N. et al. *Electro-hydraulic system architectures for MEA: comparison of central and zonal power packages*. 2018.

[63] Sinnet, M. "787 No-Bleed Systems: Saving Fuel and Enhancing Operational Efficiencies". In: *Aero Quaterly* 4 (2007), pp. 6–11. URL: www.boeing.com/commercial/aeromagazine.

[64] Torenbeek, E. *Synthesis of Subsonic Airplane Design*. Springer-Science+Business Media, B.V., 1982. ISBN: 978-90-247-2724-7.

[65] Karpuk, S. "Influence of Future Airframe and Propulsion Technologies on Energy-efficient Aircraft: Niedersächsisches Forschungszentrum für Luftfahrt - Forschungsbericht 2023-01". PhD thesis. Technische Universität Braunschweig. DOI: 10.24355/dbbs.084-202402121344-0.

[66] Kohrt, M. *Flugzeugentwurf am Beispiel einer Fokker 100*. 2001.

[67] Dorbath, F. *Luftfahrttechnisches Handbuch (LTH): Large Civil Jet Transport Statistical Mass Estimation*. 2013.

[68] Heinze, W. *Entwerfen von Verkehrsflugzeugen I*. 2023.

[69] AOPA. *DENSITY ALTITUDE*. URL: https://www.aopa.org/training-and-safety/active-pilots/safety-and-technique/weather/density-altitude.

[70] Buxbaum, J. et al. *Rolle der Automatisierung bei der Umsetzung klimaoptimierter Anflugprofile*. 2023. DOI: 10.25967/610098.

[71] Balack, P. *Integration strategies for a fuel-driven range extender on a 19-seatter battery-electric aircraft*. 2023.

[72] European Comission. *Flightpath 2050: Europe's Vision for Aviation: Report of the High-Level Group on Aviation Research*.

[73] Hoelzen, J. et al. "Hydrogen-powered aviation and its reliance on green hydrogen infrastructure – Review and research gaps". In: *International Journal of Hydrogen Energy* 47.5 (2022), pp. 3108–3130. ISSN: 03603199. DOI: 10.1016/j.ijhydene.2021.10.239.

[74] Flight International. *Bombardier costs Dash 8-400 development.* URL: https://www.flightglobal.com/bombardier-costs-dash-8-400-development/15657.article (visited on 07/21/2024).

[75] Elkind, E. *Reuse and Repower: How to Save Money and Clean the Grid with Second-Life Electric Vehicle Batteries.*

[76] Al-Alawi, M. K.; Cugley, J., and Hassanin, H. "Techno-economic feasibility of retired electric-vehicle batteries repurpose/reuse in second-life applications: A systematic review". In: *Energy and Climate Change* 3 (2022), p. 100086. ISSN: 26662787. DOI: 10.1016/j.egycc.2022.100086.

[77] Ploetner, K. O. "Operating Cost Estimation for Electric-Powered Transport Aircraft". In: *2013 Aviation Technology, Integration, and Operations Conference.* Reston, Virginia: American Institute of Aeronautics and Astronautics, 2013. ISBN: 978-1-62410-225-7. DOI: 10.2514/6.2013-4281.

[78] De Havilland Aircraft of Canada. *Airport Planning Manual: DHC-8 Series 400.* 2022.

[79] United Nations Economist Network. "Circular Economy: New Economics For Sustainably Development". In: (). URL: https://www.un.org/sites/un2.un.org/files/circular_economy_14_march.pdf (visited on 07/19/2024).

[80] United Nations. *Sustainable Development Goals: Take Action for the Sustainable Development Goals.* URL: https://www.un.org/sustainabledevelopment/sustainable-development-goals/.

[81] Atescan-Yuksek, Y. et al. "Comparative life cycle assessment of aluminium and CFRP composites: the case of aerospace manufacturing". In: *The International Journal of Advanced Manufacturing Technology* 131.7-8 (2024), pp. 4345–4357. ISSN: 0268-3768. DOI: 10.1007/s00170-024-13241-3.

[82] Haraldsson, J. and Johansson, M. T. "Review of measures for improved energy efficiency in production-related processes in the aluminium industry – From electrolysis to recycling". In: *Renewable and Sustainable Energy Reviews* 93 (2018), pp. 525–548. ISSN: 13640321. DOI: 10.1016/j.rser.2018.05.043.

[83] Hauschild, M. Z.; Rosenbaum, R. K., and Olsen, S. I. *Life Cycle Assessment: Theory and Practice.* Cham: Springer International Publishing, 2018. ISBN: 978-3-319-56474-6. DOI: 10.1007/978-3-319-56475-3.

[84] atmosfair gGmbH. "atmosfair Flug-Emissionsrechner: Dokumentation der Methode und Daten". In: (). URL: https://www.atmosfair.de/wp-content/uploads/flug-emissionsrechner-dokumentation-berechnungsmethode-1.pdf.

[85] International Air Transport Association. "IATA Sustainable Aviation Fuel Roadmap". In: (2015). URL: https://www.iata.org/contentassets/d13875e9ed784f75bac90f000760e998/safr-1-2015.pdf.

[86] Lufthansa Group. *Wieso mit Sustainable Aviation Fuel fliegen?* URL: https://lufthansa.compensaid.com/de/projects/sustainable-aviation-fuel.

[87] Lufthansa Group. *Sustainable Aviation Fuel: SAF ist eine echte Alternative zu fossilem Flugkraftstoff und essenziell für die Energiewende in der Luftfahrt.* URL: https://www.lufthansagroup.com/de/verantwortung/klima-umwelt/sustainable-aviation-fuel.html#:~:text=Beim%20Herstellungs%2D%20und%20Lieferprozess%20von,80%20reduzierten%20CO2%2DFu%C3%9Fabdruck.

[88] DLR- Institut für Verbrennungstechnik. *FAQ Sustainable Aviation Fuels (SAF).* URL: https://www.dlr.de/de/vt/forschung-transfer/faqs/faq-saf.

[89] Steinke, S. *Emirates führt virtuelle Fenster ein.* 2017. URL: https://www.flugrevue.de/zivil/neue-suiten-fuer-die-boeing-777-300er-emirates-fuehrt-virtuelle-fenster-ein/.

[90] Spakovszky, Z. S.; Chen, Y., and Greitzer, Edward, Cordero, Zachary. "A Megawatt-Class Electrical Machine Technology Demonstrator For Turbo-Electric Propulsion". In: *AIAA Aviation Forum.* Vol. 2023.

[91] Kota, S.; Flick, P., and Collier, F. S. "Flight Testing of FlexFloil TM Adaptive Compliant Trailing Edge". In: *54th AIAA Aerospace Sciences Meeting.* Reston, Virginia: American Institute of Aeronautics and Astronautics, 1042016. ISBN: 978-1-62410-393-3. DOI: 10.2514/6.2016-0036.